

8-2019

Effects of Component Model Fidelity Level on Dynamic Analysis Accuracy of a Multi-MW Wind Turbine Drivetrain

Nathaniel James Beasley
Clemson University, nbeasle@clemson.edu

Follow this and additional works at: https://tigerprints.clemson.edu/all_theses

Recommended Citation

Beasley, Nathaniel James, "Effects of Component Model Fidelity Level on Dynamic Analysis Accuracy of a Multi-MW Wind Turbine Drivetrain" (2019). *All Theses*. 3189.
https://tigerprints.clemson.edu/all_theses/3189

This Thesis is brought to you for free and open access by the Theses at TigerPrints. It has been accepted for inclusion in All Theses by an authorized administrator of TigerPrints. For more information, please contact kokeefe@clemson.edu.

EFFECTS OF COMPONENT MODEL FIDELITY LEVEL ON
DYNAMIC ANALYSIS ACCURACY OF A MULTI-MW
WIND TURBINE DRIVETRAIN

A Thesis
Presented to
the Graduate School of
Clemson University

In Partial Fulfillment
of the Requirements for the Degree
Master of Science
Mechanical Engineering

by
Nathaniel James Beasley
August 2019

Accepted by:
Dr. Gang Li, Committee Chair
Dr. Phanindra Tallapragada
Dr. Lonny Thompson

Abstract

Wind farms can incur major expenses due to turbine gearbox component failure that often occurs within five years of deployment. Turbine testing facilities such as Energy Innovation Center (EIC) in Charleston, SC are a growing resource used by the wind energy industry to improve our understanding of turbines in the field and accelerate turbine development. In the meantime, a multibody dynamics model has been developed in EIC for a mutli-MW wind turbine to carry out performance and life assessments to understand the influence of high-frequency mass and misalignment imbalance forces and gear transmission forces.

This thesis aims to investigate multibody dynamics modeling options and understand how modeling fidelity level of four components of interest influences the simulated response of the entire drivetrain under load. The components of interest were the main shaft, bed plate, first planetary carrier, and gearbox housing. The model fidelity levels of these bodies were varied from flexible body representations containing many component modes to rigid body representation with few degrees of freedom. The system was subjected to ramped unidirectional loading input at the nose of the rotor hub, which emulates testing conditions that are periodically run on drivetrains at EIC. Campbell analysis was then performed on a subsystem gearbox model to understand how component flexibility affects the speed-dependent vibration of gearbox components.

Activating more component modes was found to improve the relative accuracy in the motion of the high-speed shaft. This benefit was judged against the relative computational cost for activating each of the components' modes. The bedplate's dynamic modes had the greatest influence on the motion of the high-speed shaft. Representing all drivetrain bodies as rigid bodies leads to a significant overprediction of the internal motion and forces of the drivetrain. Activating the four components' first thirty dynamic modes caused a computational cost increase of 5 times. Carrier and gearbox housing flexibility softens the vibration frequencies of the gearbox subsystem across the turbine operating speed range. Strategic recommendations are contributed according to some differing purposes in design and testing of turbine drivetrains.

Dedication

This thesis is dedicated to my mother, my awesome example of perseverance.

Acknowledgments

I would like to thank our Clemson advisors for their guidance and instruction, and for the opportunity they offered me to participate in the valuable work being done by Clemson University SCE&G Energy Innovation Center (EIC) and General Electric (GE). It meant a great deal to have senior mentors who were both approachable and helpful whenever I needed you. The EIC team of Drs. Bibo and Panyam provided invaluable support and guidance on this project. EIC invested a wealth of quality models that jumpstarted the process of learning multibody simulation. The GE engineering team of Jim Madge and Phillippe Giguere provided critical insight to the needs and challenges facing the wind industry. As seasoned wind turbine specialists they provided excellent guidance according to their understanding of wind turbine testing and design. I appreciate the time all the project partners gave to mentor me and guide this work. This project would not have succeeded without each of your contributions. The knowledge and skills I've learned from you are invaluable assets as I start my engineering career.

Table of Contents

Title Page	i
Abstract	ii
Dedication	iv
Acknowledgments	v
List of Tables	viii
List of Figures	ix
1 Introduction	1
1.1 Motivation	1
1.2 Literature review	3
1.3 Objectives	5
2 Effect of component flexibility on displacement and modal frequency response	7
2.1 Test article: EIC reduced drivetrain model	7
2.2 Fidelity levels impacting external and internal loads	9
2.3 Investigation strategies	11
2.4 Uniform activation of component mode shapes	20
2.5 Non-uniform activation of component mode shapes	24
2.6 Drivetrain mode shape study	31
3 Effect of component flexibility on low-frequency gearbox modes .	34
3.1 Test article: standalone gearbox	34
3.2 Fidelity level and investigation strategies	36
3.3 Uniform activation of component mode shapes	41
3.4 Non-uniform activation of component mode shapes	49
4 Effect of component flexibility on gearbox risk frequency prediction	53
4.1 Campbell analysis	54

4.2	Uniform activation of component mode shapes	60
4.3	Non-uniform activation of component mode shapes	62
5	Conclusions	66
6	Future work	68
	Appendices	71
A	Natural frequency fluctuations using FE 225	72
B	Simple Multi DOF Jeffcott Rotor	75
	Bibliography	79

List of Tables

2.1	Model configurations for studying uniform mode activation	21
2.2	Overall effect of mode switching on high-speed shaft max displacement (values plotted in Figure 2.13)	23
2.3	Model configurations for studying non-uniform mode switching	25
2.4	Effect of carrier mode activation on high-speed shaft displacement (val- ues plotted in Figure 2.14)	27
2.5	Effect of Gearbox Housing mode activation on high-speed shaft max displacement (values plotted in Figure 2.15)	28
2.6	Effect of Main Shaft mode activation on high-speed shaft max displace- ment (values plotted in Figure 2.16)	29
2.7	Effect of Bed Plate mode activation on high-speed shaft max displace- ment (values plotted in Figure 2.17)	30
2.8	Summary table of results	30
2.9	System mode frequency dependence on component mode activation .	32
3.1	Model configurations for studying uniform mode activation	41
3.2	Config 2 system natural frequencies evaluated at 67 s	42
3.3	Overall effect of component mode switching on gearbox natural fre- quencies (values plotted in Figure 3.15)	48
3.4	Model configurations for studying non-uniform mode activation . . .	49
3.5	Effect of housing mode switching on gearbox natural frequencies (val- ues plotted in Figure 3.16)	51
3.6	Effect of housing mode switching on gearbox natural frequencies (val- ues plotted in Figure 3.17)	52
4.1	Order line labels	55
4.2	Model configurations for studying uniform mode activation	60
4.3	Overall effect of component mode switching on backward whirl risk frequency (values plotted in Figure 4.6)	62
4.4	Model configurations for studying non-uniform mode activation . . .	63
4.5	Effect of housing mode switching on whirl risk frequency (values plot- ted in Figure 4.7)	64
4.6	Effect of housing mode switching on whirl risk frequency (values plot- ted in Figure 4.8)	64

List of Figures

1.1	Testbench rig capable of testing wind turbines rated up to 7.5 MW (image taken from EIC website [4])	2
1.2	Comprehensive strategy to investigate wind turbine gearbox reliability (image taken from GRC plan report [3])	4
1.3	GRC preliminary model of gearbox using Simpack software [3]	5
2.1	Reduced drivetrain visualization (flexible bodies are colored, rigid bodies are gray)	8
2.2	Simplified drivetrain topology	8
2.3	EIC Simpack system topology view (flexible bodies colored orange, first stage carrier is inside gearbox assembly)	10
2.4	Side view of bed plate (solid line represents a rigid connection to the ground)	12
2.5	Main shaft mode shapes scaled up 4x (a) Front view of 1st mode-bending (b) Top view of 2nd mode- bending (c) Front view of 3rd mode- torsion	13
2.6	Top view first stage planet carrier	13
2.7	Top view gearbox housing	14
2.8	Simpack flexible body visualization	15
2.9	Daily startup external loads applied at the hub's center point	16
2.10	Back torque applied at the generator output shaft	17
2.11	High speed shaft displacement is measured by the motion of the green star relative to the red star (local coordinate axes are highlighted in yellow)	18
2.12	High-speed shaft displacement response in high fidelity vs medium fidelity configurations	19
2.13	Overall effect of mode switching on high-speed shaft max displacement	23
2.14	Effect of carrier mode activation on high-speed shaft displacement	27
2.15	Effect of Gearbox Housing mode activation on high-speed shaft max displacement	28
2.16	Effect of Main Shaft mode activation on high-speed shaft max displacement	29
2.17	Effect of Bed Plate mode activation on high-speed shaft max displacement	30
2.18	First three drivetrain system mode shapes	32

3.1	Standalone gearbox	35
3.3	Gearbox system topology view (flexible bodies colored orange)	37
3.2	Level of complexity for FE 204 compared with that of FE 14 and FE 225 [6])	38
3.4	Input torque on main carrier	39
3.5	Resulting main carrier axial rotation	40
3.6	Input conditions at first planetary carrier	40
3.7	Reverse torque applied at gearbox backend	40
3.8	Config 2 natural frequencies from linear resonance analysis	42
3.9	Mode 1 first stage thrust (1s thrust)	44
3.10	Mode 2 torsion	44
3.11	Mode 3 first stage whirl (1s whirl)	45
3.12	Mode 4 first stage planet thrust (1p thrust)	45
3.13	Mode 5 first stage carrier whirl (1c whirl)	46
3.14	Fidelity influence on gearbox natural frequencies	47
3.15	Overall effect of component mode switching on gearbox natural frequencies	47
3.16	Effect of housing mode switching on gearbox natural frequencies	51
3.17	Effect of carrier mode switching on gearbox natural frequencies	52
4.1	Gear and shaft orders	55
4.2	Conical whirl [12]	57
4.3	Output shaft forward conical whirl (red arrow is whirl direction; green arrow is shaft spin direction according to right hand rule)	58
4.4	Gyroscopic effect on whirl frequency	59
4.5	Fidelity influence on whirl excitation via pinion gear mesh	61
4.6	Overall effect of component mode switching on whirl risk frequency	61
4.7	Effect of carrier mode switching on whirl risk frequency	63
4.8	Effect of housing mode switching on whirl risk frequency	64
6.1	Example of 3D Campbell chart [7]	69
2	FE 2040 monotonic system frequency chart	73
3	FE 225 Fluctuations in 2D Campbell chart	74
4	Multi DOF [12]	75
5	Multi DOF Jeffcott rotor model	75
6	2d topology of Jeffcott rotor	76
7	Linear runup of Jeffcott rotor	77
8	Forward whirl mode shape	77
9	Backward whirl mode shape (red arrow is whirl direction; green arrow is shaft spin direction according to right hand rule)	78

Chapter 1

Introduction

1.1 Motivation

On-shore and off-shore wind energy has arisen as a major energy source for several nations. With increasing market interest the quality of design in the wind energy industry has also increased dramatically. Designers have become more knowledgeable about the true effects of wind farm field conditions on turbines. A wind turbine is a uniquely challenging system because of the dramatic difference in rotational speeds represented in various stages of the drivetrain. For example, the main driving shaft of some turbines operates ideally with input speeds on the order of 10 rpm and drives a high-speed shaft near the generator at well above 1000 rpm.

In the past 5-7 years gearbox manufacturers such as Timken have realized the potential for increasing life and performance of wind turbine drivetrains by engineering gears and bearings for wind-specific application. They have replaced gearbox components more ideally suited to industrial mill power transmissions [9]. Still there is much to learn as most gearboxes won't last more than five years before major gearbox components, or the entire gearbox needs to be replaced. The Gearbox Reliability

Database maintained by the National Renewable Energy Laboratory records that 60% of all wind turbine gearbox failures are caused by bearing failures long before the life defined by the International Organization for Standardization, and American Bearing Manufacturers Association [10].

Wind turbine testing facilities such as the Energy Innovation Center (EIC) in Charleston are a growing resource used by the wind industry to improve our understanding of turbines in the field and accelerate turbine development. EIC supports wind turbine development with advanced load testing services [5]. The facility boasts a 7.5 MW test stand and a 15 MW test stand which are designed to load and test wind turbine nacelles. The testbench is a valuable instrument that can be connected to a wind turbine nacelle and load the turbine with controlled loading in all 6 degrees of freedom (axial, vertical, lateral, tilt, yaw, torque) with capability of simulating extreme wind loading conditions. The load application unit (LAU) in Figure 1.1 is the prime mover of the testbench. It can be controlled to simulate forces and moments caused by wind loading on the rotor. The LAU enables scientists to study even the rarest wind events that may be prohibitively difficult to reliably reproduce in field studies.

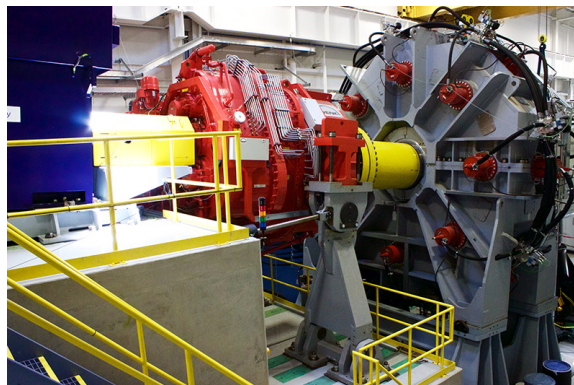


Figure 1.1: Testbench rig capable of testing wind turbines rated up to 7.5 MW (image taken from EIC website [4])

The testbench is coupled with the Duke Energy eGRID (Electrical Grid Research Innovation and Development) also housed at EIC. The 15-MW hardware-in-the-loop grid simulator supports education, research and economic development to speed new electrical technologies to market. The eGRID can simulate the electrical grid of any country in the world. The work being done at EIC in collaboration with industry partners is accelerating the development and deployment of new wind turbine technology, while reducing the cost of energy and growing the wind market. Toward that end EIC has also built advanced multibody simulation (MBS) models to extend the capabilities of the center in parallel with studies being performed on the testbench. Often the same controller settings are even extracted from the testbench controls system for use in the MBS system. Scientists at EIC and industry partners came together to formulate several student projects to support further MBS model development, including the present study.

1.2 Literature review

There is a long history of progressive modeling focused on capturing wind turbine loads. Large collaborations especially with such groups as NASA and NREL [3] have encouraged information sharing that greatly benefits current research. The Gearbox Reliability Collaborative (GRC) identified a generic deficiency in current wind turbine bearing performance (generic meaning pervasive across turbine brands and regions). The 3-point plan summarized in Figure 1.2 has been implemented to trace the root cause of deficient gearbox life.

The GRC report [3] identified unique failures in wind turbine gearboxes that have not been susceptible to some solutions successfully applied in other industrial bearing applications. Analytical methods available at that time for assessing bearing

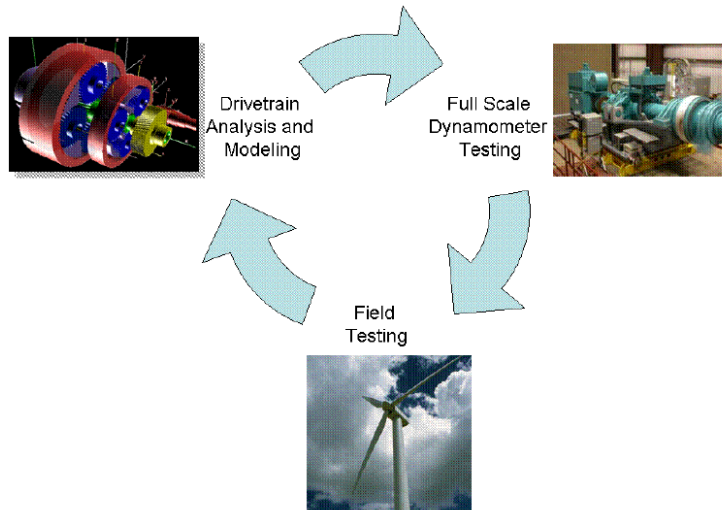


Figure 1.2: Comprehensive strategy to investigate wind turbine gearbox reliability (image taken from GRC plan report [3])

life had insufficient accuracy to help. Their plan moving forward involved the use of Simpack as the multibody software of choice for drivetrain modeling, especially for its ability to represent the geometry and stiffness properties of the gearbox housing, shafts, bearings, and gears; these components will be shown to be integral parts of the present study as well.

A GRC turbine model has since been investigated to understand the influence of component fidelity on measured responses of interest. It was found that artificial rigid connections exhibited greater error in high-speed events. Furthermore, the rigid models were found to over-predict the bearing loads by about 20%. That gearbox includes only two stages, one planetary and one helical, which differs from the gearbox investigated in this work. The GRC model doesn't investigate the influence of a flexible base structure or carrier.

Coupled FEA-MBS techniques were used by Heege et al. to account for dynamic effects to improve design and specification of turbine gearboxes. Heege suggests

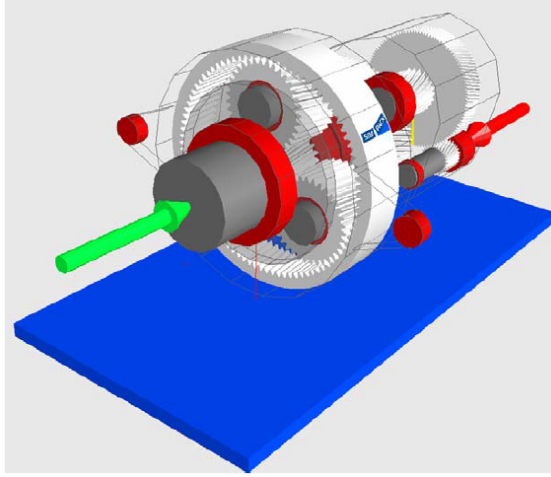


Figure 1.3: GRC preliminary model of gearbox using Simpack software [3]

that this coupled approach is required for obtaining turbine loads due to the non-linear and three-dimensional character of wind turbine dynamics [8]. Helsen et al. agreed with Heege and proceeded to introduce FEA models to a three-stage MBS gearbox model with attention to how the FEA model interfaced with inputs/outputs from MBS bodies. They found significant improvement in predicting the overall modal response of a turbine system when upgrading a turbine model from a rigid main carrier to a main carrier with FEA representation [2].

Beyond the GRC collaboration, some sophisticated bearing models have been contributed which consider non-linearity induced by bearing clearance, gear tooth separation and variation in mesh stiffness [11]. Planet bearing clearance was found to affect the bearing tooth loads leading to chaos.

1.3 Objectives

The broadest goal of this project to document the relationship between fidelity level and modeling accuracy, and develop modeling strategies that will allow

individual components to be incorporated into an entire drivetrain sub-system model. This thesis will explain the methods and findings and demonstrate the utility of multi-body modeling for wind turbine applications. A more accurate representation of drive train components improves the assessment of system performance and life. The components of the system, and how to model them, are not only important for designing the architecture of the turbine but are also important for predicting component loads, dynamic behavior and durability. This study investigates *relative* performance of different modeling strategies. These models inevitably simplify the actual behavior of a wind turbine. Experimental validation of the various drivetrain models will be one of the most important tasks listed in the future work chapter for continuing model improvement. The next section describes the first steps of identifying modeling fidelity options according to their influence on loads internal or external to the turbine gearbox. Proceeding chapters will describe how these fidelities were implemented and the correlations that were developed between accuracy and fidelity.

Chapter 2

Effect of component flexibility on displacement and modal frequency response

2.1 Test article: EIC reduced drivetrain model

EIC modeling specialists developed a model of a multi-MW platform drivetrain. Figure 2.1 is a visualization of that Simpack drivetrain model consisting of major components including the bed plate, main shaft, gearbox, high speed shaft coupling and generator. Interfacing components are used to make external connections on the drivetrain with the testbench and foundation.

Simpack force elements and joints govern the many connections between drivetrain components. Most of these bodies are modeled as rigid except for the structural components; the bed plate, gearbox housing, main shaft, and first planetary stage carrier (main carrier). These flexible components are reduced finite element bodies generated using component mode synthesis (CMS). The system diagram in Figure

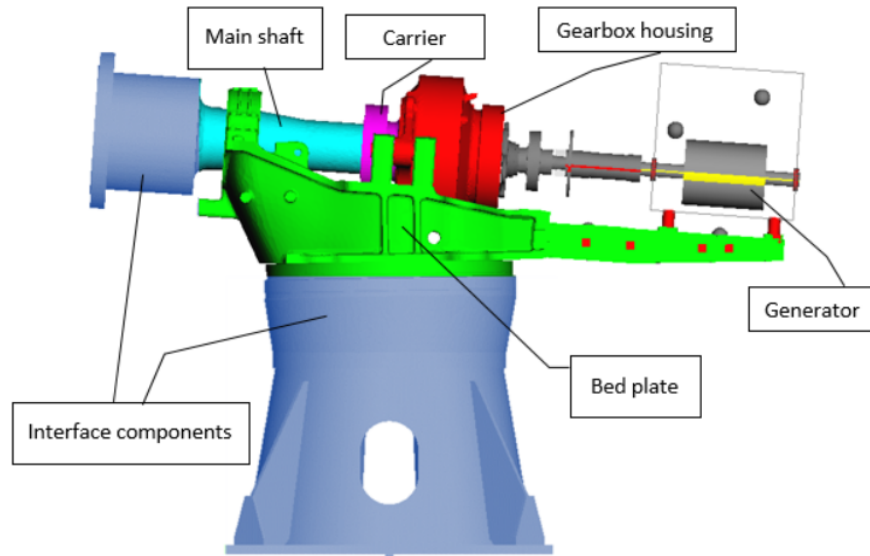


Figure 2.1: Reduced drivetrain visualization (flexible bodies are colored, rigid bodies are gray)

2.3 shows the full connectivity description of the model. But Figure 2.2 is sufficient to describe the system components and connections at a high level.

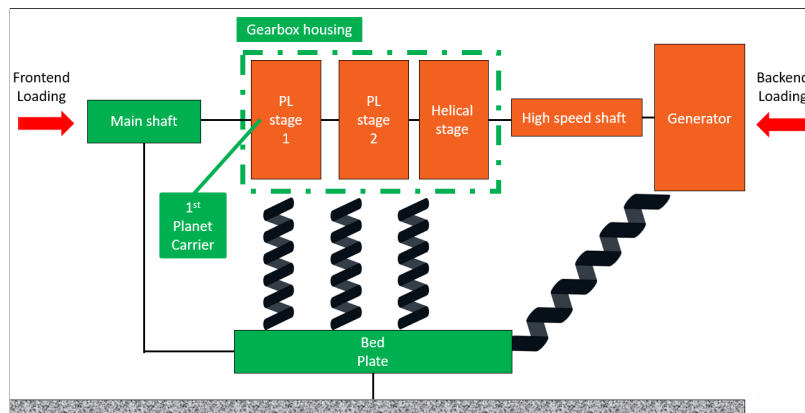


Figure 2.2: Simplified drivetrain topology

Simpack flexible bodies exhibit various orders of bending and torsion according to the number of component mode shapes that are activated. The reduced flexible models can be suppressed to activate as few as 0 modes (which would effectively turn

a flexible body into a rigid body) or as many as 30 dynamic modes. The bed plate supports the main shaft through a revolute joint and supports the gearbox housing and the generator using bushing elements.

2.2 Fidelity levels impacting external and internal loads

The term “fidelity” will be used to describe alternative MBS modeling methods or modeling elements that affect the accurate calculation of a wind drivetrain’s displacement and force responses to wind loads. Generally, a higher fidelity method or element will return greater accuracy in exchange for paying a greater computational expense in solve time. The accuracy of FEA and MBS (and coupled FEA-MBS) models generally increases when more degrees of freedom are used in the model. More degrees of freedom can be introduced in the form of more sophisticated modeling elements representing gears and bearings, the number of dynamic modes for representing elastic motion of constituent elements, the number of FE elements used, etc. An important question to be answered is whether a given model fidelity is reliable enough for various purposes such as component choice, design and failure analysis, etc. It is not necessarily true that a more sophisticated drivetrain model should be preferred. A model that serves all these necessary purposes at an acceptable computational cost will be preferable for design flexibility and more rapid implementation of wind turbines.

The modeling approach taken in this project takes stock of two sources of loading experienced by the drivetrain and support structure:

- External forces from the rotor or load application unit (LAU) with frequencies

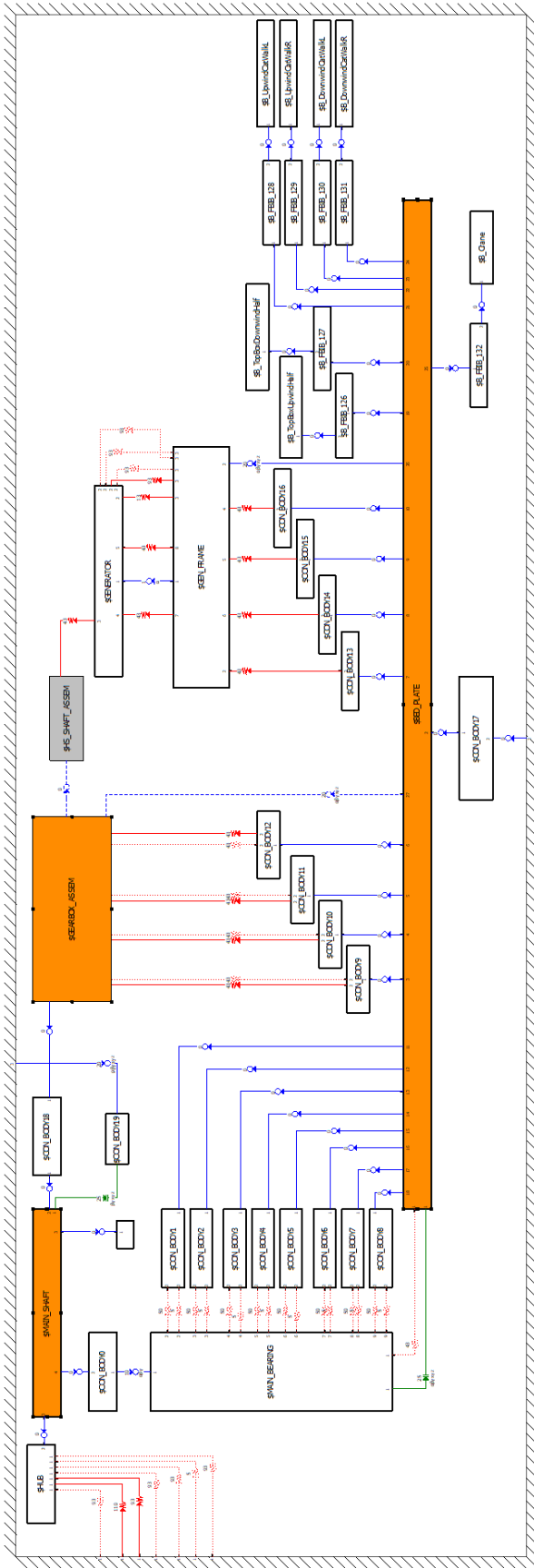


Figure 2.3: EIC Simpack system topology view (flexible bodies colored orange, first stage carrier is inside gearbox assembly)

from 0.2-10 Hz

- Internal forces
 - Forces due to mass and misalignment imbalance within the drivetrain with higher frequency than rotor forces
 - Gear transmission forces with higher frequencies than rotor forces

Two aspects of drivetrain model fidelity were identified for investigation. Separate studies sought to investigate whether improving these two aspects of fidelity would significantly improve model predictions both internal and external to the gearbox. First the influence of flexibility was studied by changing the number of active modes in the simulations and comparing the response of the high-speed shaft. This study will provide an understanding of the sensitivity of the rotor response external to the gearbox to structural fidelity. Flexible bodies can improve the model with the capacity to predict elastic motion of components, which cause real misalignments that affect mechanical life. Second, the existing simple gearbox components were replaced with progressively more sophisticated gear and bearing modeling elements. This study will provide an understanding of the response inside the gearbox to the choice of gear and bearing descriptions.

2.3 Investigation strategies

In the field, the drivetrain and support structure experience external loading from rotor loads at a relatively low frequency (0.2-10 Hz). These input loads have been observed to cause deflections in the physical drivetrain components leading to shaft and gear misalignments. Since the rigid body drivetrain could not replicate this elastic motion, modeling specialists at EIC produced FE models of four drivetrain

components. The bed plate, main shaft, first stage planet carrier, and gearbox housing were chosen because they play a significant role in transmitting external loads. Short descriptions of each of these bodies are given below.

2.3.1 Bed plate

The bed plate is bolted to the ground at its base, and supports all the other drivetrain members above it.

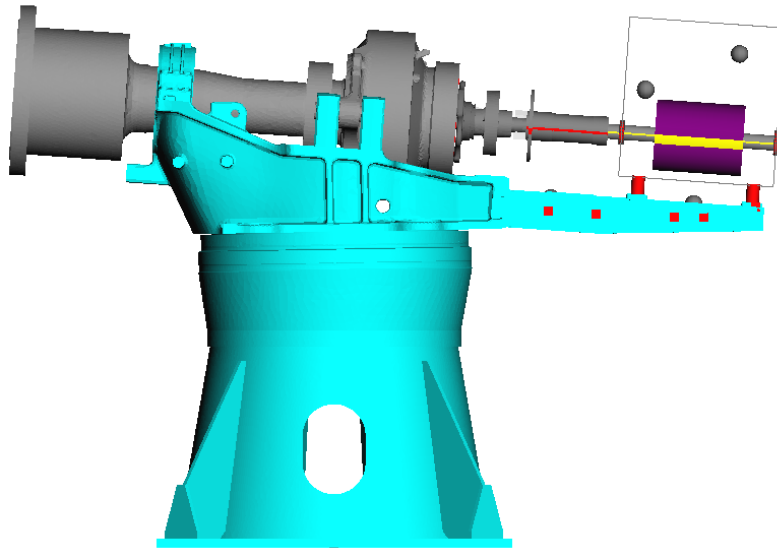


Figure 2.4: Side view of bed plate (solid line represents a rigid connection to the ground)

2.3.2 Main shaft

The main shaft is the prime mover to the rest of the reduced drivetrain supported by the main bearing, which is itself fixed to the bed plate through a revolute joint, and the carrier.

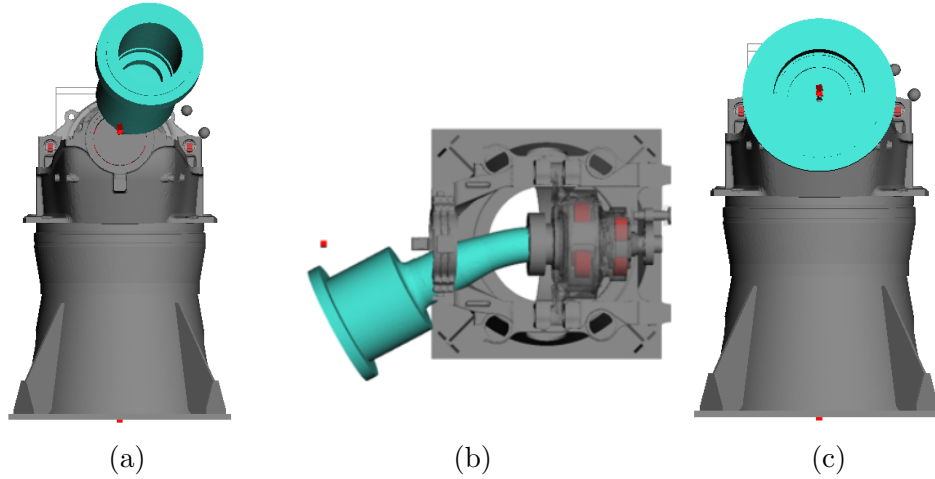


Figure 2.5: Main shaft mode shapes scaled up 4x (a) Front view of 1st mode- bending (b) Top view of 2nd mode- bending (c) Front view of 3rd mode- torsion

2.3.3 First stage planet carrier

The first stage planet carrier is so-called because it “carries” each of the planetary gears as they mesh between inside a ring gear, and mesh against a centrally located sun gear. The carrier is driven by the main shaft and transmits to the rest of the drivetrain through the planetary gears. The drivetrain has two such planetary stages, with the first planetary stage actuating the second planetary stage in series.

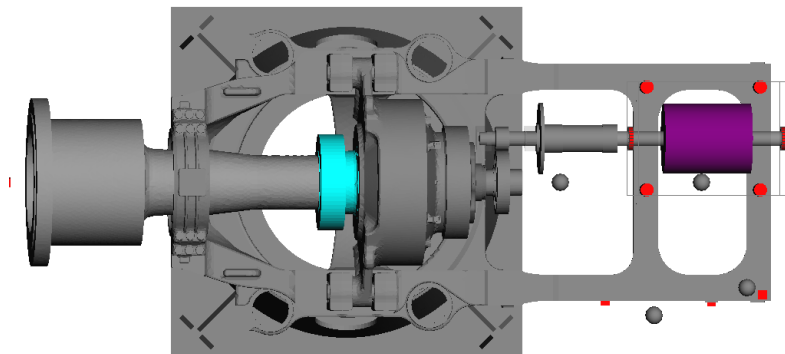


Figure 2.6: Top view first stage planet carrier

2.3.4 Gearbox housing

The gearbox housing is supported by the bed plate on the housing’s two cylindrical arms. The housing is a structural body that “houses” the components of the first and second planetary stages. The rotation of the main shaft is transmitted through the first and second stages, which progressively lower the torque and increase the rotational speed. The second stage sun shaft feeds out from backend of the housing to the parallel gear stage, through the high-speed shaft to the generator.

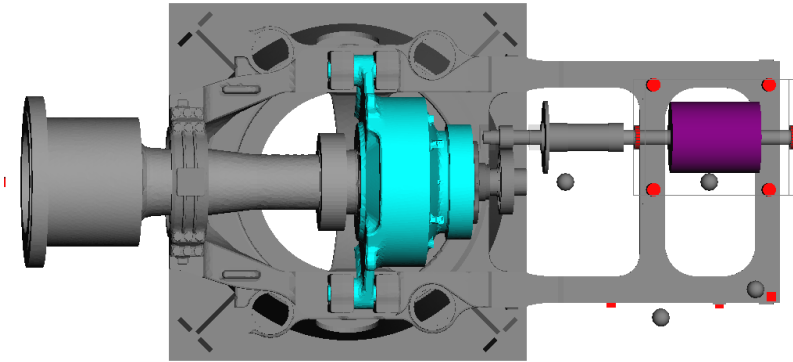


Figure 2.7: Top view gearbox housing

The flexible components in Simpack are reduced FE models generated using CMS (see Figure 2.8). CMS requires a choice of how many modes to use to keep in the reduced flexible body. The most realistic model will include an infinite amount of modes, but practical considerations such as computational cost will limit the number of modes extracted. Designers decided that 30 modes would be sufficient for this study. Those modes capture high-order bending and torsion motion in each body. The CMS models were imported to Simpack to create flexible bodies and connected via the master degrees of freedom to the other rigid members of the drivetrain.

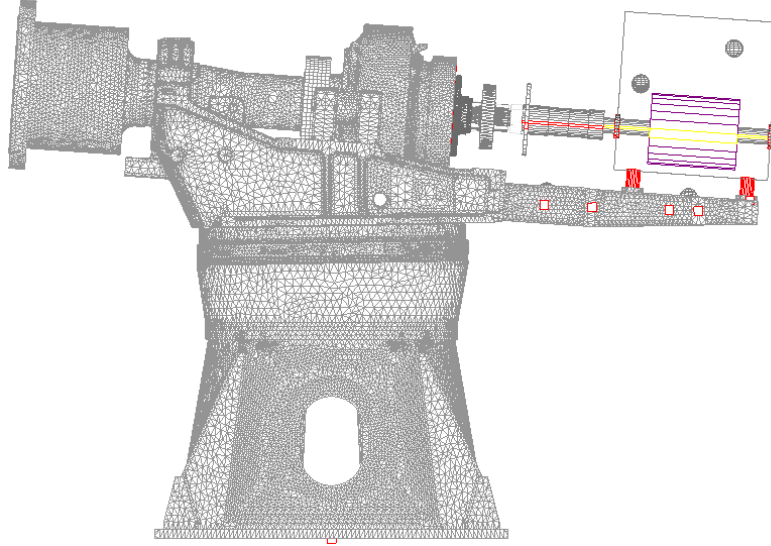


Figure 2.8: Simpack flexible body visualization

2.3.5 Applied loads

After the model construction was complete the next step was to choose what loads to apply to the drivetrain. Since the model does not include the rotor blades, the main shaft was driven by an input torque ramped up from rest to maintain a rotation of 14.3 rpm (this is a typical rated speed for multi-MW turbine platforms). Turbine drivetrains also experience non-torque wind loading. These winds cause both forces and moments at the blades, which are transmitted via the rotor hub to the main shaft. A dynamic load profile could have been applied at the rotor hub to emulate wind loads measured in the field. But a simpler load was chosen to establish a basic understanding of how the flexible turbine components respond to each hub load type and direction.

The unidirectional loading profile depicted in Figures 2.9 and 2.10 was applied to the turbine hub. This 9.5 min load sequence has been termed the “daily startup”

profile by EIC as it is used in their labs to warm up turbine drivetrains. The applied loads have been normalized in the figures below due to the proprietary nature of this testing sequence. Ramping forces are applied sequentially in three directions before bending moments are applied. The loadset applies a torque resisting the rotor motion at the generator end.

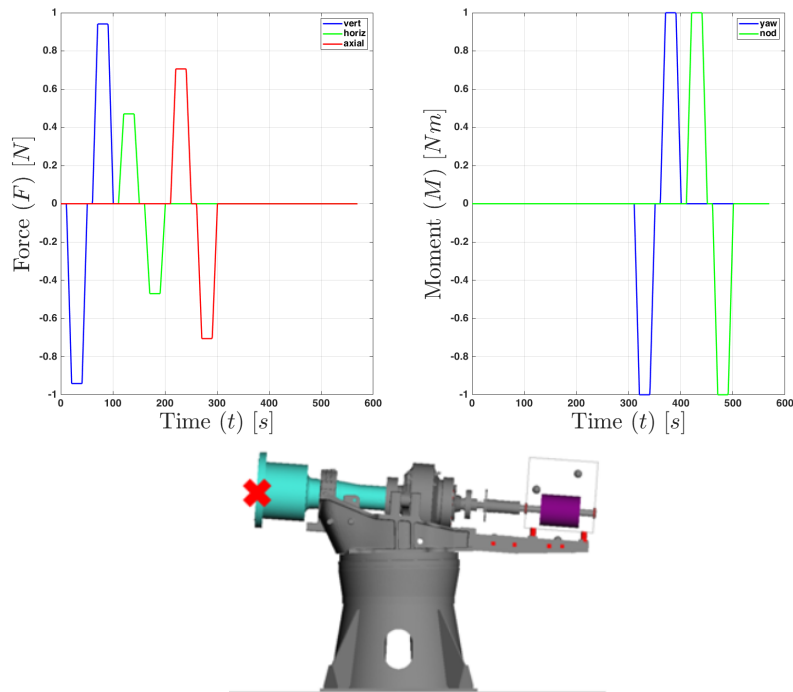


Figure 2.9: Daily startup external loads applied at the hub's center point

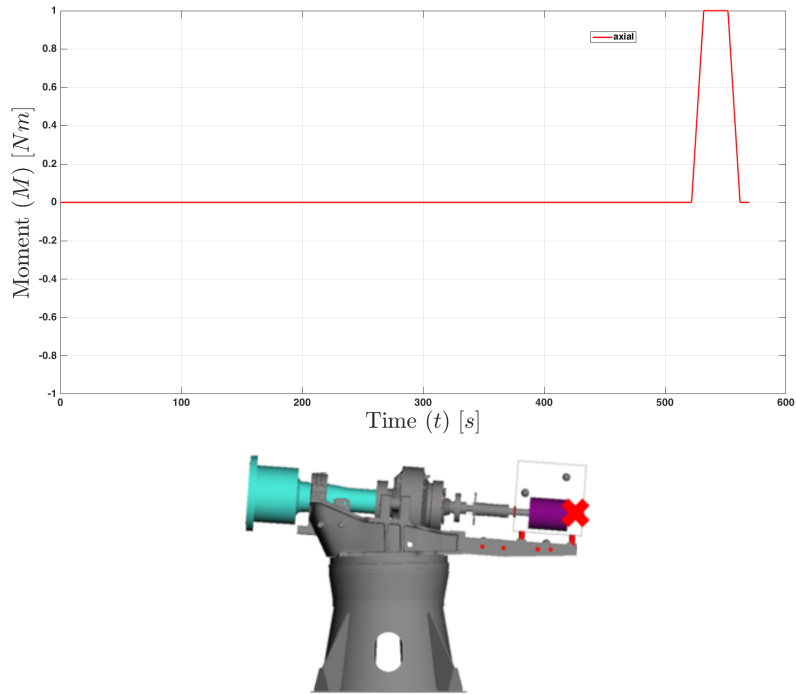


Figure 2.10: Back torque applied at the generator output shaft

2.3.6 Response of interest

To simplify the analysis, only the response of the high-speed shaft was considered in this study. The response was measured by tracking the displacement of the high-speed shaft relative to the generator frame as show in Figure 2.12. This response point is especially interesting because it captures the global motion of the gearbox and indicates misalignment between the generator and the gearbox.

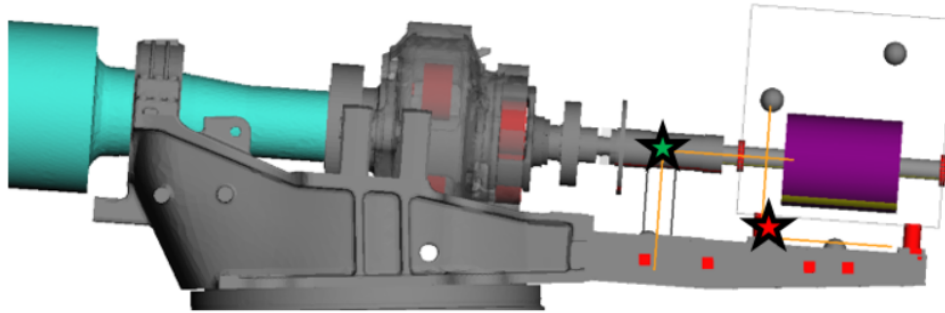


Figure 2.11: High speed shaft displacement is measured by the motion of the green star relative to the red star (local coordinate axes are highlighted in yellow)

Simulation results in proceeding studies were compared to find the difference in their highest peaks values. The difference in peak values is a simple measure that captures the effect of component flexibility. This method reduces time-history displacements such as those in Figure 2.12 to max values in axial, horizontal, and vertical displacement. A benchmark simulation should be chosen as a reference point. In this case the “all 30” mode configuration was the reference case, and all other configurations’ displacement peaks are compared to this reference.

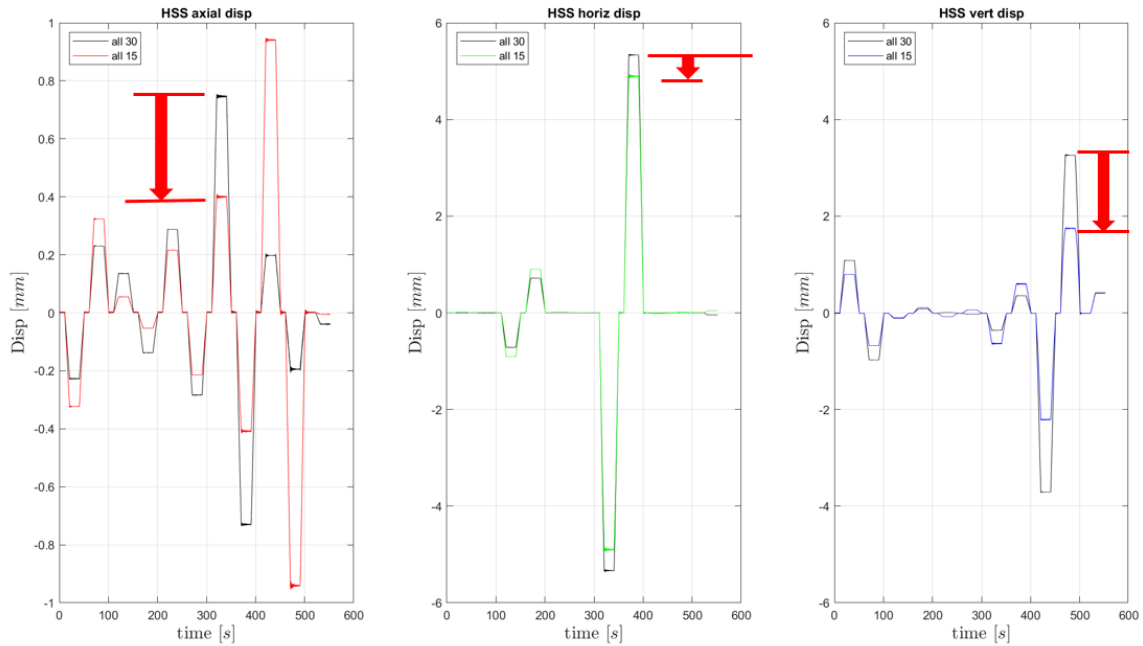


Figure 2.12: High-speed shaft displacement response in high fidelity vs medium fidelity configurations

Another output of interest is the time factor, which is a convenient measure for comparing the relative cost of simulations. Time factor is defined as the dimensionless ratio between the real solve time (wall time) to the simulated time in the model.

$$\text{time factor} = \frac{\text{real solve time}}{\text{simulated time}}$$

For example, if it takes 100 real-time sec for a computer to solve a drivetrain model that simulates a 10 sec dynamic event, the model is said to execute with a time factor of 10. In this study the same computer was used to run all the simulations and the computer run conditions were the same, so time factor values can be directly compared (Intel Core i7-4790 CPU @ 3.60 GHz, 8 CPUS).

2.3.7 Fidelity level investigation strategies

Two studies were undertaken related to structural fidelity. The first study considered four configurations of the Simpack drivetrain. Each configuration uniformly varied the amount of active mode shapes available to flexible bodies between low, medium, high fidelities. The number of modes activated in each component was 0, 15 and 30 in each configuration, respectively. The study documents the basic influence of fidelity on model performance. The second study is similar to the first except that the component mode shapes were activated *non-uniformly*. Each configuration assigned high fidelity to all components except for one component of interest that was varied between low, medium, and high fidelity. This study looks beyond the basic influence of structural fidelity to compare the independent influence of each component and its modal content.

2.4 Uniform activation of component mode shapes

This study set out to characterize the influence of structural fidelity on the motion of the drivetrain. The motivation of the study was to learn how many modes is sufficient to produce realistic results without significantly degrading the model. Computational costs were estimated to judge the performance trade-off between accuracy and solution time. Several “configurations” were prepared to answer these questions, each of which progressively lowered the modes available to the four flexible bodies. The system models were subjected to ramping unidirectional forces and moments to observe how the fidelity of the primary components affected the system’s internal displacements and solve times.

2.4.1 Simulation procedure

The EIC model was used to make four model configurations that varied in the active modes available to each of four major components: the bed plate, main shaft, main carrier, and gearbox housing. Note that all components exhibited similar mode shapes for the lowest three modes (configuration 2) corresponding to first bending, second bending, and torsional modes (Figure 2.5). The lowest fidelity configuration was prepared in Simpack by activating the first three modes for each body, and deactivating the 4th-30th modes. This caused the bodies to exhibit the equivalent flexible behavior they would have if CMS had been conducted with 3 modes rather than 30. The medium fidelity configuration had its lowest 15 modes active, but deactivated the 16th-30th modes. The rigid case (no active modes) was run as a reference case, even though it's already been noted that this configuration cannot exhibit elastic motion. The bodies within a given configuration had the same number of active modes to observe the overall effect of mode activation.

Table 2.1: Model configurations for studying uniform mode activation

<i>Config</i>	Bed plate	MS	Carrier	GBX
1		0 modes		
2		3 modes		
3		15 modes		
4		30 modes		

Several system-level modeling choices were applied to the configurations in the same way. The planetary gear stages were all modeled using a gear-ratio element that simplified gear motion to a simple torque transfer (see Chapter 3 for a discussion of more sophisticated gear representations). Bearings were all represented with single degree of freedom rotational joints. The torque arm elastomers supporting the gearbox were represented by modeling elements with translation and rotational damping

and stiffness, as well as clearance.

A standard model preparation was required before useful measurements could be taken. The system was first brought to static equilibrium using the built-in Simpack equilibrium solver. Next the main shaft was accelerated with a controlled torque that ramped the axial rotational speed to a steady state of 14.3 rpm. The running system could then be studied under loading from various forces and moments. Outputs of interest were judged based on how much their peaks varied from that of the 30-mode high-fidelity configuration (configuration 4). First the maximum displacement in the configuration 4 graphs was identified. Then the concurrent maximum displacements in the other three configurations were recorded. The difference in concurrent peak values is a simple measure that captures the effect of mode activation.

2.4.2 Results

Recall that the 30-mode configuration is assumed to be the true response of the system. Reading Figure 2.13 right-to-left shows that the overall effect of reducing the flexible modes of the four bodies is to underestimate the true radial displacement¹. Thrust deflection (axial) is not affected nearly as much. The radial underestimate is more severe in configuration 2 compared to configuration 3, although the degradation happens at different rates. The slope of the line stepping from 30 to 15 modes is greater in the vertical direction. But the slope of the line stepping from 15 to 3 modes is greater in the horizontal direction. The vertical direction graph degrades in a linear fashion compared to the horizontal trend which has a much more distinct knee at 15 modes.

¹X-direction is another name for axial, y-direction is horizontal, z-direction is vertical. 'Mzn' denotes an input moment at the hub about the z-axis (vertical axis) in the negative direction. 'Myp' is a positive input moment about the y-axis.

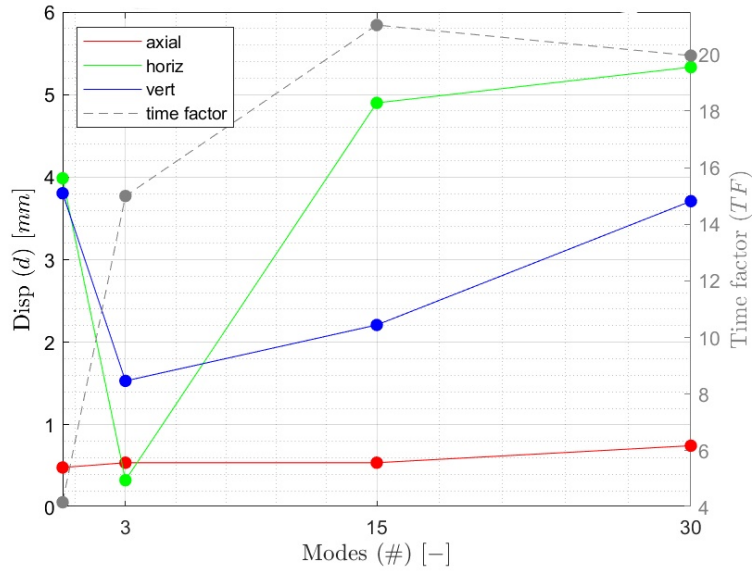


Figure 2.13: Overall effect of mode switching on high-speed shaft max displacement

Table 2.2: Overall effect of mode switching on high-speed shaft max displacement (values plotted in Figure 2.13)

Config	Bed plate	MS	Carrier	GBX	Time factor	HSS max axial disp		HSS max horiz disp		HSS max vert disp	
						Cause	Disp [mm]	Cause	Disp [mm]	Cause	Disp [mm]
1					4.18	'Mzp'	0.48	'Mzn'	3.99	'Myp'	3.81
2					14.80	'Mzn'	0.57	'Mzn'	0.33	'Myp'	1.53
3					21.04	'Myp'	0.54	'Mzn'	4.90	'Myp'	2.21
4					19.96	'Myn'	0.75	'Mzp'	5.34	'Myp'	3.71

Surprisingly, the rigid body configuration was not a poor estimate of the true displacement response of the system. In general, this may not be the case, especially when the gear fidelity is increased (see chapter 3) and it may not be the case when the turbine is loaded with dynamic inputs, rather than ramped unidirectional forces and moments. With respect to the 3-mode configuration, the rigid configuration was an overestimate of the max displacement.

Figure 2.13 demonstrates the trade-off between fidelity and solve time. There is a 5x cost increase to upgrade from configuration 1 to configuration 4. The computational cost of configuration 4 is 25% greater than that of configuration 2. The time

factor at 15 modes was surprisingly greater than the time factor at 30 modes, but this was likely an anomaly. The models were solved on a laptop where background tasks and other local conditions can disrupt resources available to Simpack. A larger sample size of simulations might reveal that the average time factor for configuration 3 is less than that of configuration 4, but these results suggest that the difference is probably negligible.

Solve time is also strongly dependent on the system under consideration. Systems with nonlinear behavior, greater degrees of freedom, longer simulation time, higher sample rate, and more fluctuating inputs and responses will require more resources to solve. This simulation had steady or linearly ramped inputs and only simulated 9.5 min at a sample rate of 100 Hz. Simulation expense considerations will become more significant when the modeling application requires several long simulations run in parallel.

2.5 Non-uniform activation of component mode shapes

The preceding study introduced flexible members to the drivetrain to observe to whether the additional computational expense is a good investment. It was appropriate to analyze a small set of uniform mode configurations to answer this question. However, this approach does not provide a fundamental understanding of how each flexible member contributes to the motion of the entire drivetrain. It's not clear whether any component's flexibility is more significant than others, or to what extent the elastic motion of several components interacts. The preceding study takes the next step by isolating and ranking the influence of each components' structural

fidelity.

2.5.1 Simulation procedure

The methodology of this study is very similar to that of the uniform mode activation study. The reduced drivetrain model was prepared using the same procedure: selecting certain active modes for four bodies, bringing the system to static equilibrium, ramping up to 14.3 rpm etc. The same outputs of interest from the previous study were captured to quantify model response, but more configurations were required to measure the independent influence of each body’s structural fidelity. The structural fidelity of one body was varied while holding the others constant to isolate the contribution of a single body’s flexibility. A large variance in model response will suggest that structural fidelity of that body plays a major role, while a low variance suggests a minor role. Listed below are the relevant configurations.

Table 2.3: Model configurations for studying non-uniform mode switching

<i>Config</i>	Bed plate	MS	Carrier	GBX
<i>1</i>	0	0	0	0
<i>4</i>	30	30	30	30
<i>5</i>	3	30	30	30
<i>6</i>	15	30	30	30
<i>7</i>	30	3	30	30
<i>8</i>	30	15	30	30
<i>9</i>	30	30	3	30
<i>10</i>	30	30	15	30
<i>11</i>	30	30	30	3
<i>12</i>	30	30	30	15

The configuration numbering introduced in the previous study is continued in this study, so configuration 4 is the same model previously referred to as the high-fidelity model. These configurations can be grouped into pairs according to the

component that is being varied. For example, configurations 5 and 6 vary the bed plate active modes while keeping a high level of active in the other components. This pair was used to perform a case study of the bed plate, and similar studies were performed for each component using configuration pairs {7,8}, {9,10} and {11,12}.

2.5.2 Results

Most components revealed a similar trend found in the previous study. As flexibility decreases, the max displacement at the high-speed shaft decreases. Introducing higher modes to the carrier had the opposite effect on high-speed shaft motion. Figure 2.17 shows how switching bed plate modes affects high-speed shaft displacement. The displacement values have a high variance at the three mode settings. The displacement values at each mode setting in Figure 2.17 are already very similar to that of Figure 2.13, showing that bed plate is the most significant flexible body affecting motion at the high-speed shaft. This is probably because its flexibility motion directly moves the generator frame. The carrier and gearbox housing modes have significantly less influence on high-speed shaft and solve time compared to the main shaft and bed plate. The 3 to 15 mode switch made a more significant change in max high-speed shaft displacement for all flexible components except for the gearbox housing. The gearbox housing saw its most dramatic change in the 15 to 30 mode switch. It's not clear that there is a trend in component flexing influencing thrust (axial) deflection.

The dynamic interaction of many components is responsible for the system's motion. The method in this study can be misleading because it only considers the independent influence of each body. A more complete understanding of the system may be revealed by a full factorial analysis that involves switching the modes of more

than one component at a time to see what, if any, interaction effects are observed between the flexible bodies.

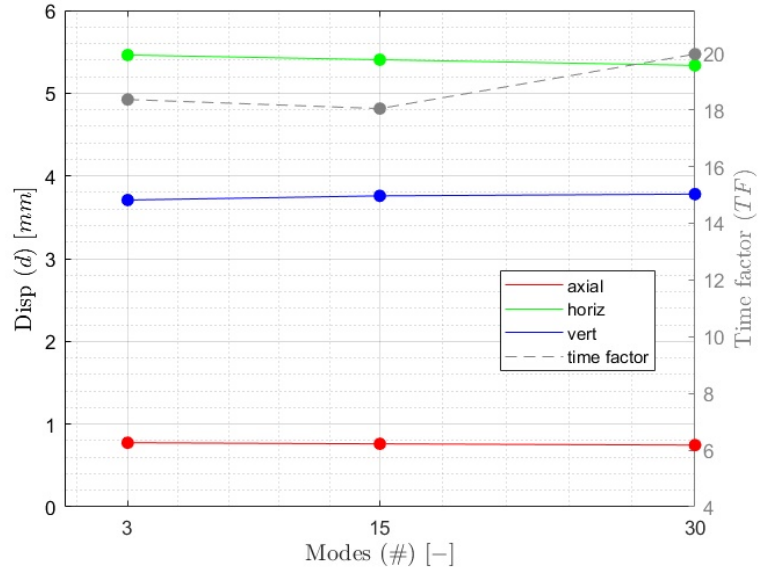


Figure 2.14: Effect of carrier mode activation on high-speed shaft displacement

Table 2.4: Effect of carrier mode activation on high-speed shaft displacement (values plotted in Figure 2.14)

Config	Bed plate	MS	Carrier	GBX	Time factor	HSS max axial disp		HSS max horiz disp		HSS max vert disp	
						Cause	Disp [mm]	Cause	Disp [mm]	Cause	Disp [mm]
1	0	0	0	0	4.18	'Mzp'	0.48	'Mzn'	3.99	'Myp'	3.81
9	30	30	3	30	18.36	'Mzn'	0.78	'Mzp'	5.46	'Myp'	3.76
10	30	30	15	30	18.04	'Mzn'	0.76	'Mzp'	5.40	'Myp'	3.78
4	30	30	30	30	19.96	'Myn'	0.75	Mzp'	5.34	'Myp'	3.71

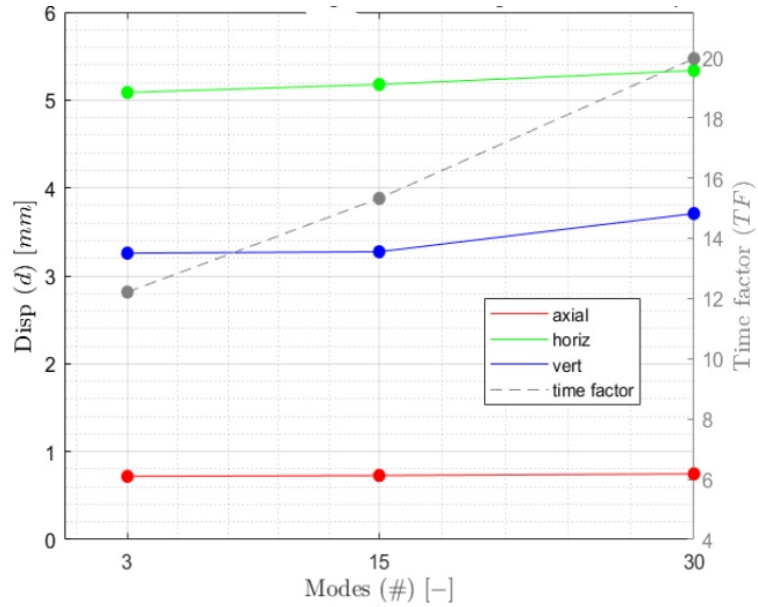


Figure 2.15: Effect of Gearbox Housing mode activation on high-speed shaft max displacement

Table 2.5: Effect of Gearbox Housing mode activation on high-speed shaft max displacement (values plotted in Figure 2.15)

Config	Bed plate	MS	Carrier	GBX	Time factor	HSS max axial disp		HSS max horiz disp		HSS max vert disp	
						Cause	Disp [mm]	Cause	Disp [mm]	Cause	Disp [mm]
1	0	0	0	0	4.18	'Mzp'	0.48	'Mzn'	3.99	'Myp'	3.81
11	30	30	30	3	12.21	'Mzn'	0.72	'Mzp'	5.09	'Myp'	3.26
12	30	30	30	15	15.32	'Mzn'	0.73	'Mzp'	5.18	'Myp'	3.27
4	30	30	30	30	19.96	'Myn'	0.75	'Mzp'	5.34	'Myp'	3.71

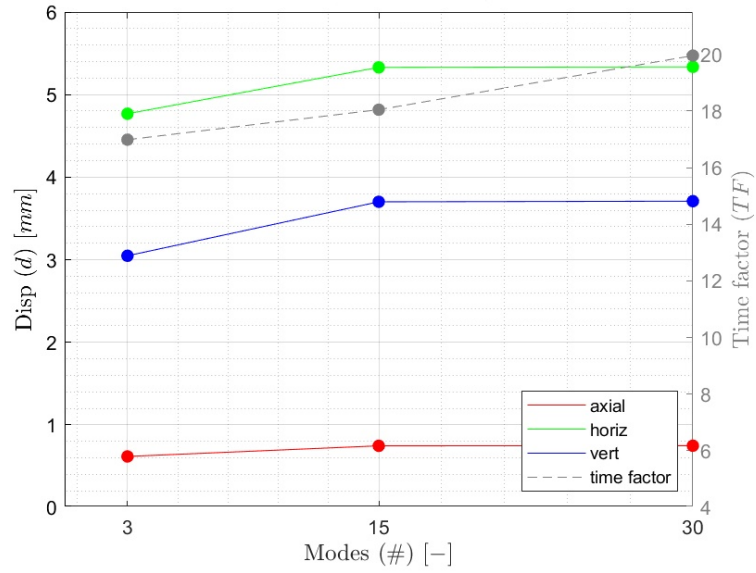


Figure 2.16: Effect of Main Shaft mode activation on high-speed shaft max displacement

Table 2.6: Effect of Main Shaft mode activation on high-speed shaft max displacement (values plotted in Figure 2.16)

Config	Bed plate	MS	Carrier	GBX	Time factor	HSS max axial disp		HSS max horiz disp		HSS max vert disp	
						Cause	Disp [mm]	Cause	Disp [mm]	Cause	Disp [mm]
1	0	0	0	0	4.18	'Mzp'	0.48	'Mzn'	3.99	'Myp'	3.81
7	30	3	30	30	16.99	'Mzn'	0.62	'Mzp'	4.77	'Myp'	3.05
8	30	15	30	30	18.05	'Mzn'	0.75	'Mzp'	5.33	'Myp'	3.70
4	30	30	30	30	19.96	'Myn'	0.75	'Mzp'	5.34	'Myp'	3.71

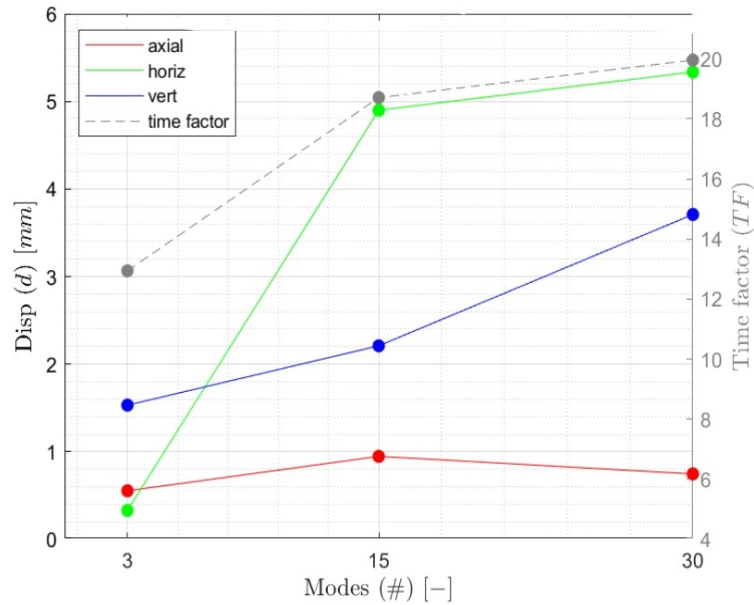


Figure 2.17: Effect of Bed Plate mode activation on high-speed shaft max displacement

Table 2.7: Effect of Bed Plate mode activation on high-speed shaft max displacement (values plotted in Figure 2.17)

Config	Bed plate	MS	Carrier	GBX	Time factor	HSS max axial disp		HSS max horiz disp		HSS max vert disp	
						Cause	Disp [mm]	Cause	Disp [mm]	Cause	Disp [mm]
1	0	0	0	0	4.18	'Mzp'	0.48	'Mzn'	3.99	'Myp'	3.81
5	3	30	30	30	12.94	'Myn'	0.55	'Mzn'	0.35	'Myp'	1.56
6	15	30	30	30	18.71	'Myn'	0.95	'Mzp'	4.96	'Myp'	2.20
4	30	30	30	30	19.96	'Myn'	0.75	'Mzp'	5.34	'Myp'	3.71

Table 2.8: Summary table of results

Config	Bed plate	MS	Carrier	GBX	Time factor	HSS max axial disp		HSS max horiz disp		HSS max vert disp	
						Cause	Disp [mm]	Cause	Disp [mm]	Cause	Disp [mm]
1	0	0	0	0	4.18	'Mzp'	0.48	'Mzn'	3.99	'Myp'	3.81
4	30	30	30	30	19.96	'Myn'	0.75	'Mzp'	5.34	'Myp'	3.71
5	3	30	30	30	12.94	'Myn'	0.55	'Mzn'	0.35	'Myp'	1.56
6	15	30	30	30	18.71	'Myn'	0.95	'Mzp'	4.96	'Myp'	2.20
7	30	3	30	30	16.99	'Mzn'	0.62	'Mzp'	4.77	'Myp'	3.05
8	30	15	30	30	18.05	'Mzn'	0.75	'Mzp'	5.33	'Myp'	3.70
9	30	30	3	30	18.36	'Mzn'	0.78	'Mzp'	5.46	'Myp'	3.76
10	30	30	15	30	18.04	'Mzn'	0.76	'Mzp'	5.40	'Myp'	3.78
11	30	30	30	3	12.21	'Mzn'	0.72	'Mzp'	5.09	'Myp'	3.26
12	30	30	30	15	15.32	'Mzn'	0.73	'Mzp'	5.18	'Myp'	3.27

2.5.3 Summary

This study demonstrates that introducing flexible bodies does influence the displacement response of the drivetrain and the model solve time. Increasing modeling fidelity from low to high will add 25% computational cost. However, decreasing structural fidelity of major drivetrain components has the effect of underestimating the magnitude of displacement at the high-speed shaft by as much as 94%. The preferred structural fidelity will depend on the application. For example, a turbine designer may value the quick estimates provided by low-fidelity models of design alternatives. Later stage design may be better suited for incorporating high-fidelity flexible body models.

The flexing of the bed plate is the most influential flexible body followed by the main shaft, gearbox housing, and finally the carrier. Activating the carrier and gearbox up to 15 flexible modes captures the elastic motion of those bodies quite well, but the main shaft and bed plate gain significant accuracy by increasing to 30 modes. The cost of increasing bed plate fidelity from low to high comes at a 54% time factor increase, compared to the main shaft's 17% time factor increase or the carrier's 9% time factor increase.

2.6 Drivetrain mode shape study

A preliminary study considered how flexibility of drivetrain components influences the modal response of the reduced drivetrain. Configurations 2-4 were equilibrated with gravity absent any input forcing. The system was solved for its stationary eigen modes and eigen frequencies reported below.

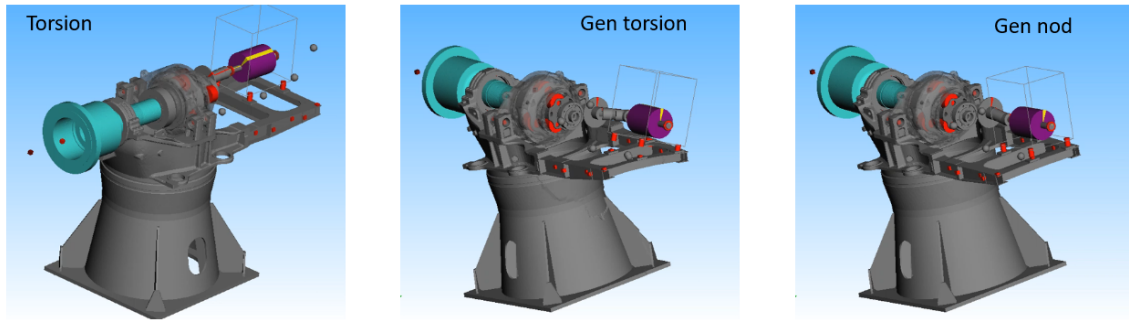


Figure 2.18: First three drivetrain system mode shapes

Table 2.9: System mode frequency dependence on component mode activation

MS	Bed plate	GBX housing	Carrier
1,...,3	1,...,3	1,...,3	1,...,3

mode #	Frequency [Hz]	Type
1	1.935	Torsion
2	3.324	Gen torsion
3	4.140	Gen nod
4	7.042	Gen frame yaw
5	7.645	Gen frame vert shear
6	9.139	Gen frame horiz shear
7	10.774	System yaw
8	11.114	System nod
9	13.267	Gen ext + nod
10	16.065	HSC extension

MS	Bed plate	GBX housing	Carrier
1,...,15	1,...,15	1,...,15	1,...,15

mode #	Frequency [Hz]	Type
1	1.877	Torsion
2	3.298	Gen torsion
3	3.895	Gen nod
4	6.886	System yaw
5	7.078	System nod
6	7.174	System nod 2
7	7.832	Gen frame vert shear
8	9.109	Gen frame horiz shear
9	12.738	Gen nod 2
10	16.052	HSC extension

MS	Bed plate	GBX housing	Carrier
1,...,30	1,...,30	1,...,30	1,...,30

mode #	Frequency [Hz]	Type
1	1.832	Torsion
2	3.273	Gen torsion
3	3.879	Gen nod
4	6.166	System yaw
5	6.819	Gen frame yaw
6	7.092	System nod
7	7.743	Gen frame vert shear
8	9.085	Gen frame horiz shear
9	12.520	Torsion + extension (system)
10	14.868	Torsion + yaw (system)

The overall influence of increasing active modes is a frequency reduction in the system's modal frequencies. For example, increasing from 3 to 30 modes for all components results in a 0.103 Hz reduction in the drivetrain first torsional frequency. Figure 2.18 shows that the torsional mode exhibits rotational motion at the main shaft, inside the gearbox, and throughout the drivetrain. The same pattern of re-

ducing eigen frequencies is observed at virtually all modes that the configurations share. Increasing model fidelity also causes some mode shapes is to distribute motion previously isolated to one area of the drivetrain throughout the system. Also, some new mode shapes appear in high fidelity models. For example, mode 4 in the config 3 chart in Table 9 is “System yaw” whereas config 2 only exhibited generator frame yaw at its 4th mode. In general, some form of the config 2 mode shapes appear in config 3 and 4 in the same order separated by several new modes shapes.

The low-frequency modal response in the turbine is sensitive to flexibility but this preliminary study does not illuminate rotor modes in and around the gearbox. The modes were dominated by low-frequency vibrations of the bed plate. Gearbox vibrations deserve to be isolated and studied for their sensitivity to model fidelity. A modal study of the current gearbox would be premature because it is modeled with simple joint bearings and torque-transfer gear meshes. While the current gearbox model is an improvement on a one-dimensional torsion model, the gearbox deserves to be developed more before performing further modal analysis. A new gearbox was constructed with advanced rotor elements to carry forward the study of turbine model fidelity.

Chapter 3

Effect of component flexibility on low-frequency gearbox modes

3.1 Test article: standalone gearbox

Chapter 2 was a system-level study that made several simplifying assumptions about the gearbox such as representing gears as torque-transfer bodies, and bearings as rigid joints. Yet the gearbox is one of the most important subsystems of any wind turbine. High fidelity representations of rotors and bearings are desirable because they reveal vibrations that significantly affect component life. Nathan Beasley and Jesalkumar Thakkar developed a high-fidelity gearbox model (the model presented here was updated with better bearing definitions and correct filtering on the main carrier body modes) [1]. That gearbox is shown in Figure 3.1 composed of two planetary gear stages and one parallel stage populated with planet carriers, shafts, gears, and bearings. The housing and main carrier bodies retain CMS processed flexible representations (see section 2.3.4 and 2.3.3). The proceeding study focused on the gearbox model isolated from the rest of the turbine drivetrain to investigate

the role of component flexibility on gear and shaft vibration. Those vibrations were divided into low frequency vibrations in the first planetary stage, and high-frequency vibrations at the output stage.

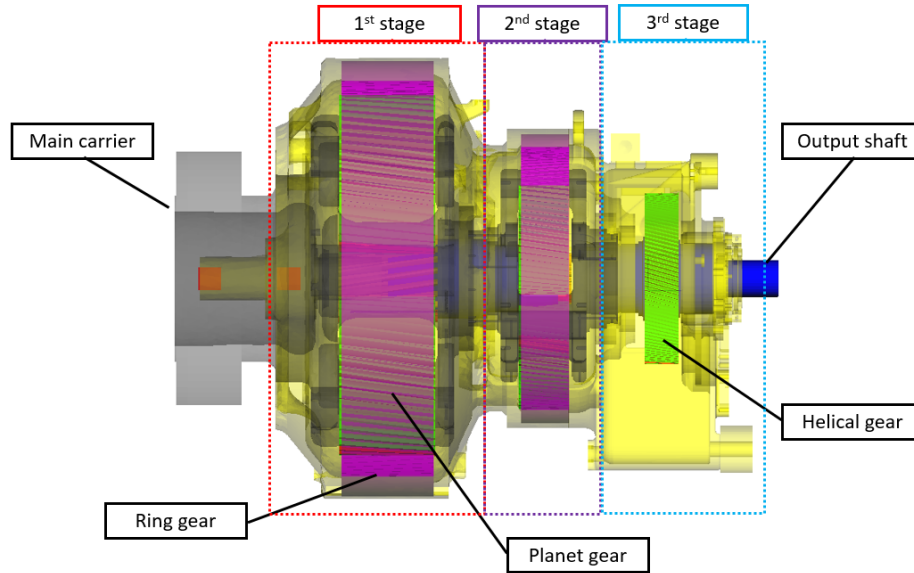


Figure 3.1: Standalone gearbox

Figure 3.3 illustrates the connection scheme within the gearbox. The leftmost cluster of bodies represents the first stage, the second cluster the second stage, and the rightmost three boxes represent the third parallel gear stage. The long slender boxes at the bottom of the diagram are the front and back bodies of the housing. Each body is connected to its neighbors at connecting points that can restrict motion to as few as 0 DOF (fixed connection). The output shaft of each gear stage transmits to the input shaft of the next stage by a fixed connection. For example, the sun shaft of the first stage is rigidly connected to the second stage carrier. Force elements feed into the left side and right sides of the diagram representing the controlled torque inputs. The left side element drives the main carrier, and the right side element drives a torque on the backend that resists the motion of the parallel stage.

Two gearing models are available in this model that can be switched, providing more gear mesh detail as it is required (gear modeling will be discussed further in the next section). All shafts, gears, and carriers are oriented along the upwind-downwind direction and these bodies are held by two bearings, one upwind and one downwind.

3.2 Fidelity level and investigation strategies

3.2.1 Gear and bearing fidelity

The lowest fidelity options in Simpack for modeling a gear mesh are FE 57 Planetary gear and FE 14 Gearbox Torque-Torque Component that represent gears as simple torque-transfer relations for planetary and parallel gear meshes, respectively. Legacy gearbox models at EIC used these torque transfer elements to represent meshing between the planet-sun, planet-ring and helical-pinion gears. Figure 3.2 lists readily available gear modeling options. Gear elements designated *FE 204: basic gear pair* and *FE 225: gear pair* are specifically recommended for wind turbine transmission applications modeling torque transmission as well as mesh stiffness.

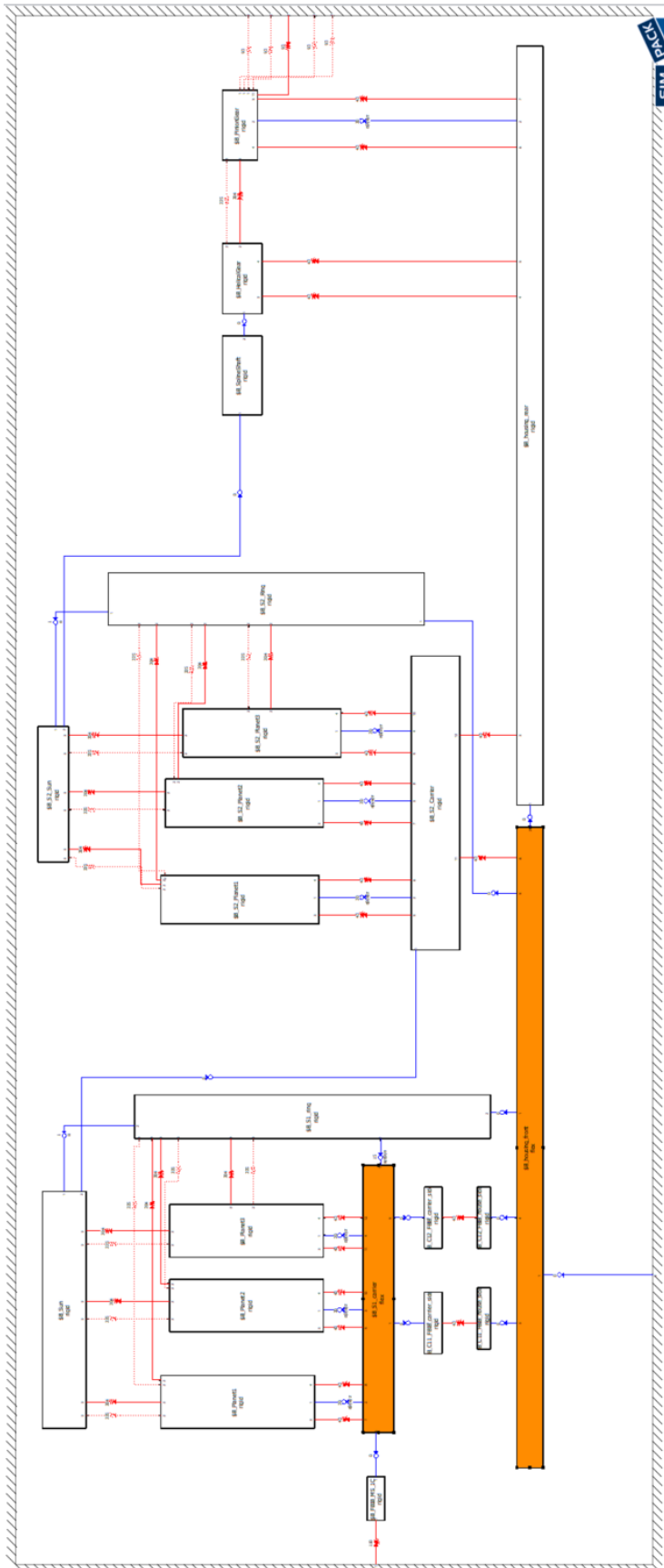


Figure 3.3: Gearbox system topology view (flexible bodies colored orange)

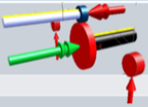
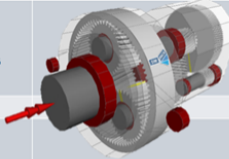
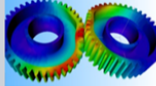
Level of fidelity ↓	Element	Characteristics	Use	
	Torsional Spring-damper (FE 14)	Applied torques Support Arm Forces	<ul style="list-style-type: none"> • 1D torsional analysis • Simplified gearbox for NVH driveline analysis 	
	Basic Gear Pair (FE 204)	+ Circumferential contact force		
	Basic Gear Pair Advanced (FE 204)	+ Radial / axial contact forces + Dynamic contact normal + Dynamic backlash	<ul style="list-style-type: none"> • NVH without mesh excitations • 3D gear shift analysis 	
	Gear Pair (FE 225)	+ Individual tooth contact + Meshing excitation + Flank modifications	<ul style="list-style-type: none"> • NVH incl. mesh excitations • Gear whine • Gear rattle 	
Flexible Gear Pair (FE 225)	+ 3D tooth and wheel dynamic deformation and resonance effects	<ul style="list-style-type: none"> • NVH • Micro geometry optimization with deformed wheels 		

Figure 3.2: Level of complexity for FE 204 compared with that of FE 14 and FE 225 [6])

FE 204 provides three-dimensional modeling of the contact normal direction allowing for dynamic modeling of backlash and pressure and helix angle [6]. Power loss due to friction can be specified but this feature was not used since friction information was not readily available. FE 225 is an appealing alternative because it extends the FE 204 element by modeling meshing excitation and gear micro geometry effects. FE 204 elements can reveal *risk frequencies* due to gear mesh excitation, but FE 225 elements can be used in a 3D Campbell analysis to detect and diagnose conditions where gear mesh excitation *actually* occurs. Unfortunately, FE 225 elements seemed to be one of the causes for some unexplained frequency fluctuations so 3D Campbell analysis was not carried out (see Appendix A).

Bearings are represented as a general spring element designated *FE 43: Bushing* parameterized with stiffness and damping in three transnational and three rotational directions. Displacements of the shafts, gears, and carriers from their zero-

positions will activate restoring forces generated by bearing force elements. The stiffness and damping of the second stage carrier and planet bearings were assumed to be the same as those of the first stage. The bearings in the parallel stage were assumed to have the same stiffness and damping as the planet bearings.

3.2.2 Applied loads

A PI controller was used to apply a driving torque to the main carrier sufficient to smoothly ramp its rotational speed from 0 rpm to 16 rpm. The max speed of 16 rpm was chosen because it slightly exceeds the rated speed of the turbine. An exponential sweep could have been chosen rather than a linear sweep, and an exponential runup would have been more computationally efficient but a linear runup was chosen because it was simpler to implement. Figure 3.4 shows that the carrier executed rotation that closely matched the speed profile prescribed by the controller.

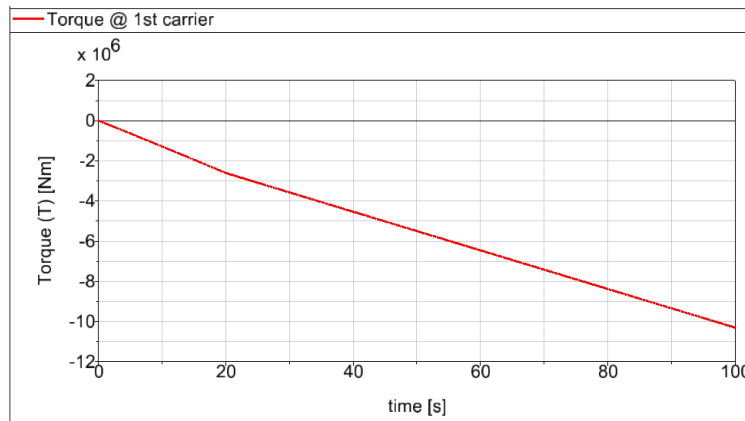


Figure 3.4: Input torque on main carrier

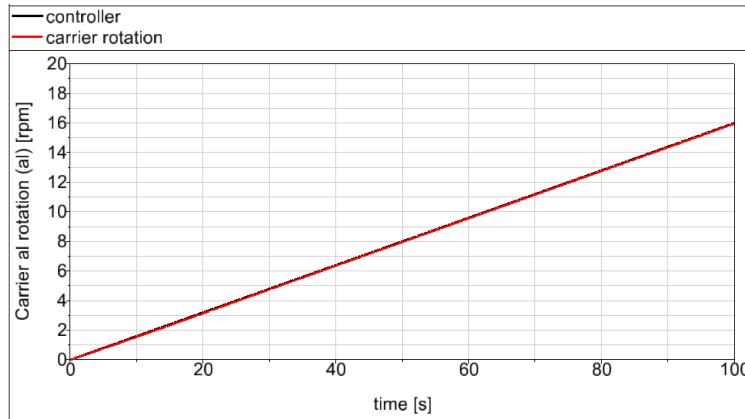


Figure 3.5: Resulting main carrier axial rotation

Figure 3.6: Input conditions at first planetary carrier

The torque shown in Figure 3.7 was applied to the backend of the gearbox at the same time the main carrier was being runup. The reverse torque ramps up over 20 s to a peak value (see Figure 2.10)¹. Note that this back torque is three orders of magnitude smaller than the main carrier torque, which is likely why the choice of back torque rampup time (20, 50, 100 s) did not cause a significant difference in the outputs of interest.

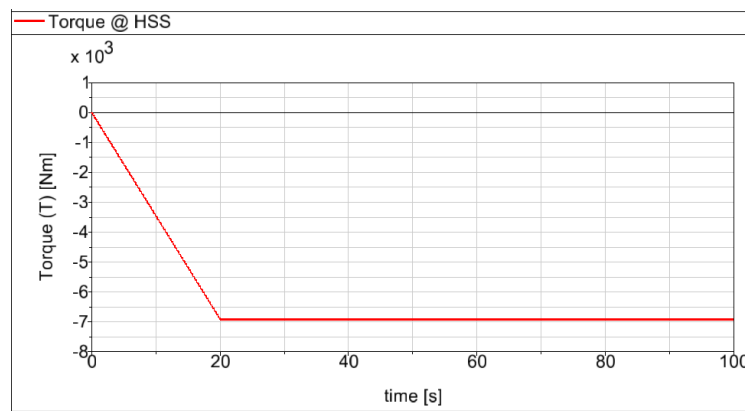


Figure 3.7: Reverse torque applied at gearbox backend

¹The negative torque applied at the main carrier is reversed to the positive direction at the third stage, so a resisting torque at the third stage should indeed be negative

3.3 Uniform activation of component mode shapes

3.3.1 Simulation procedure

The standalone gearbox was given four configurations summarized in Table 3.1 that progressively activated body modes in the main carrier and housing up to a high-fidelity configuration with 30 active modes. For similar reasons as the previous turbine system study, uniformly changing the model fidelity will reveal the overall influence of model fidelity on the output of interest. Each configuration was first equilibrated with gravity absent any torques. Then each model was runup to 16 rpm over 100 s by rotating the main carrier against a resisting torque on the output shaft.

Table 3.1: Model configurations for studying uniform mode activation

<i>config</i>	<i>fidelity</i>	# Carrier modes	# HSG modes
1	Rigid	0	0
2	Low	3	3
3	Medium	15	15
4	High	30	30

The drivetrain response was sampled at a rate of 7476 Hz to ensure that motion was captured even at $5 \times f_{max}$ where $f_{max} = 1495$ Hz is the meshing frequency between the pinion and helical gears. A Simpack linear resonance analysis script published by Dassault was configured and run on each configuration. The script calls the Simpack eigenvalue tool to evaluate the natural frequencies of the system once every second during the runup. These natural frequencies can be plotted against the carrier's rotation to find speed-dependent modes (discussed further in section 4.1). The five lowest-frequency modes will be compared between configurations to understand the influence of model fidelity.

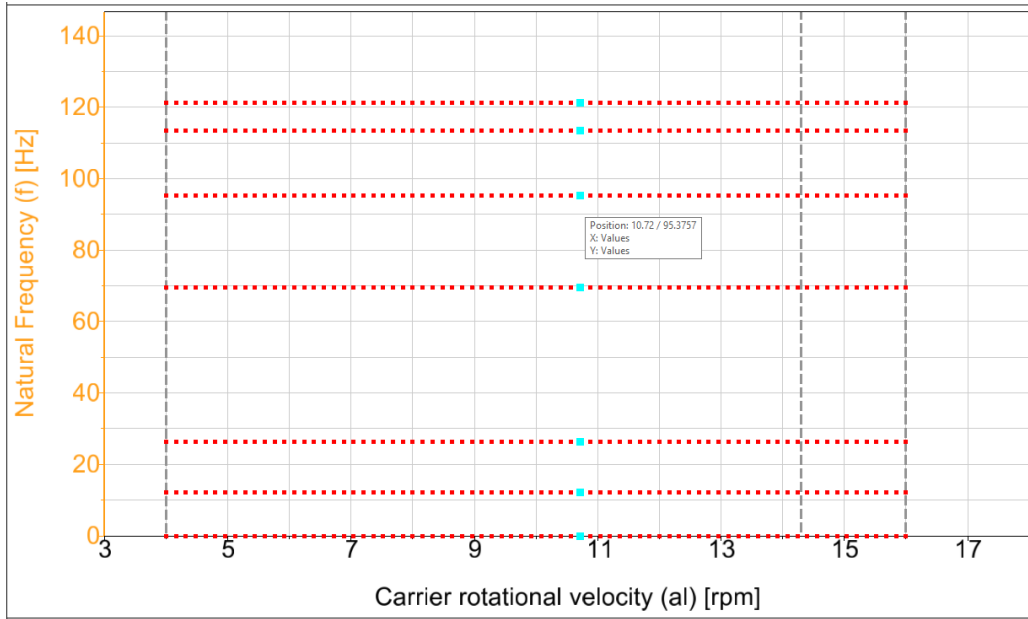


Figure 3.8: Config 2 natural frequencies from linear resonance analysis

Table 3.2: Config 2 system natural frequencies evaluated at 67 s

#	Nat Freq [Hz]
1	12.11
2	26.31
3	69.61
4	95.37
5	113.47

Figure 3.8 plots the results of the linear resonance analysis. Each red marker represents a system natural frequency that was captured at one second in time during the runup simulation. Most modes did not change their frequency over time, so their markers form a horizontal line across the chart. A column of markers represents a snapshot of the system’s natural frequencies when the carrier is moving at a particular

speed. For example, the highlighted column of natural frequencies in Figure 3.8 were evaluated at time $t = 67$ s. The system frequencies at $t = 67$ s correspond to a carrier rotational velocity of $\Delta\dot{\alpha} \times \frac{t}{\Delta t} = 16\text{rpm} \times \frac{67\text{S}}{100\text{S}} = 10.72\text{rpm}$ (the carrier has a constant acceleration).

3.3.2 System mode shapes

A total of 55 non-rigid system modes were observed in a fully flexible gearbox (after the rigid body modes were removed). The low-frequency modes showed predominant motion in the first planetary stage. Figure 3.9 shows the first natural frequency which is a transnational mode where the main carrier and first stage planets oscillate in phase on their bearings along the drive axis. The second natural frequency (Figure 3.10) is torsion of the transmission components.

This study focused on the lowest five modes listed in increasing order of frequency. Some of these modes show up in pairs that exhibit the same basic mode shape, and with very similar frequencies, but in opposite directions. For example, a whirling mode may appear twice- once with clockwise sense and a second time with counterclockwise sense. Mode 3 in Figure 3.11 shows first stage whirl moving counterclockwise at a frequency of 69.58 Hz in configuration 2, but there was also a clockwise first stage whirl mode measured at 69.63 Hz. Mode 5 depicted in 3.13 shows counterclockwise main carrier whirl at a frequency of 113.47 Hz in configuration 2, and a clockwise main carrier whirl was measured next at 113.52 Hz. In this chapter modes that have opposite direction pairs will be represented by a single mode to simplify the analysis. This is reasonable because model fidelity was found to have roughly the same effect on these mode pairs (no gyroscopic effect).

Mode 1 shown in Figure 3.9 is a vibration of the main carrier thrusting *in*

phase with the first stage planet gears.

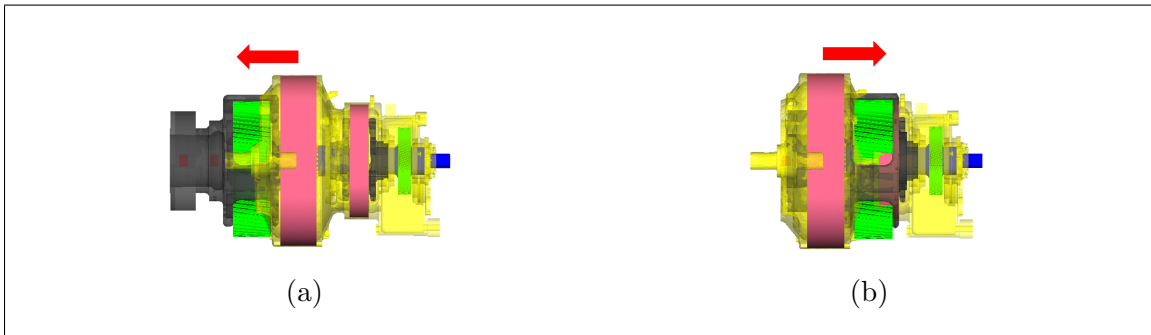


Figure 3.9: Mode 1 first stage thrust (1s thrust)

Mode 2 shown in Figure 3.10 is a torsional mode of all the shafts and gears in the gearbox. Visualized above by the rotation of a red arrow fixed to the sun gear.

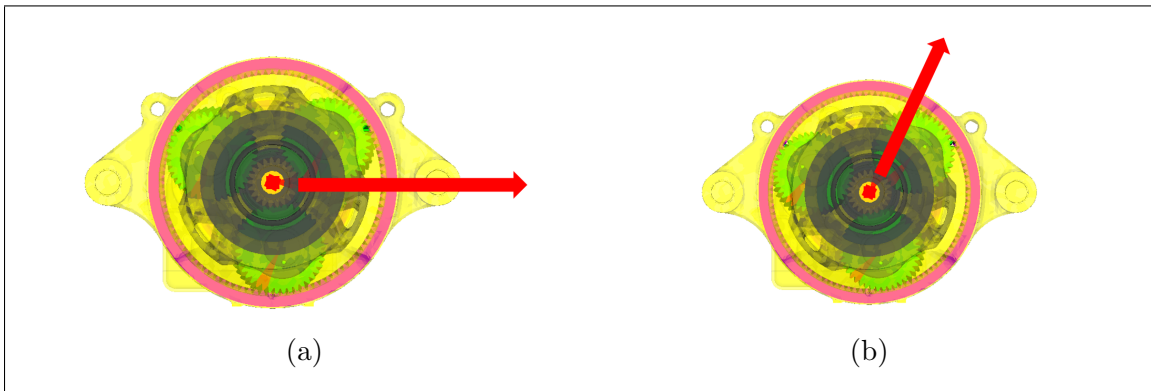


Figure 3.10: Mode 2 torsion

Mode 3 shown in Figure 3.11 is a relatively large whirling mode of the first planetary stage that also thrusts the planet gears.

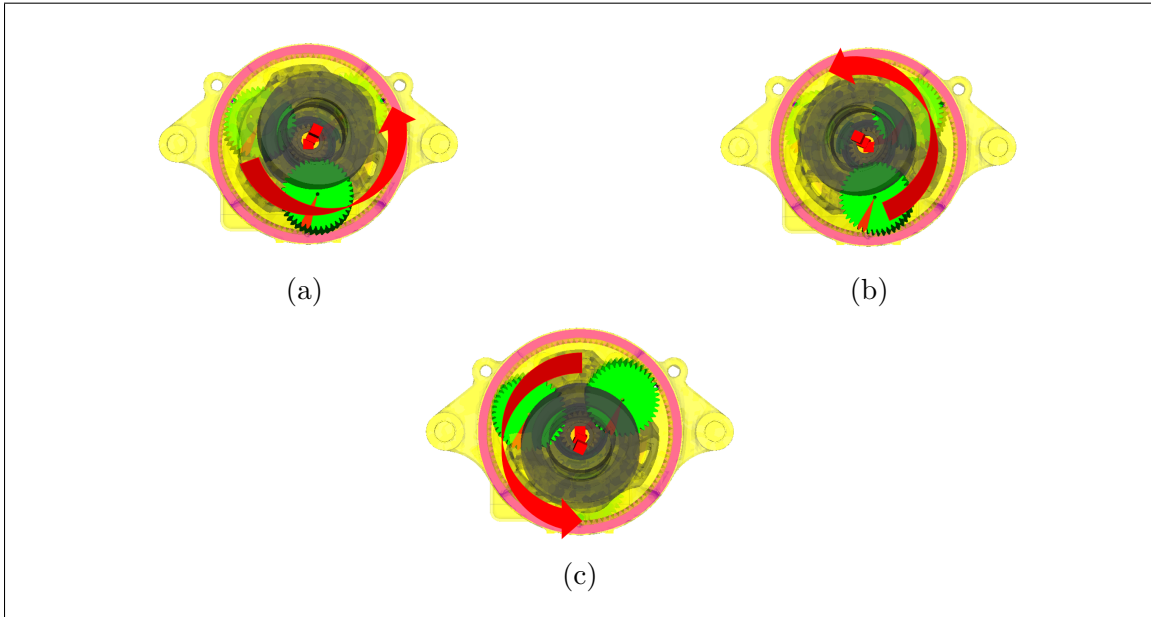


Figure 3.11: Mode 3 first stage whirl (1s whirl)

Mode 4 shown in Figure 3.12 is a vibration of the main carrier thrusting *out of phase* with the first stage planet gears.

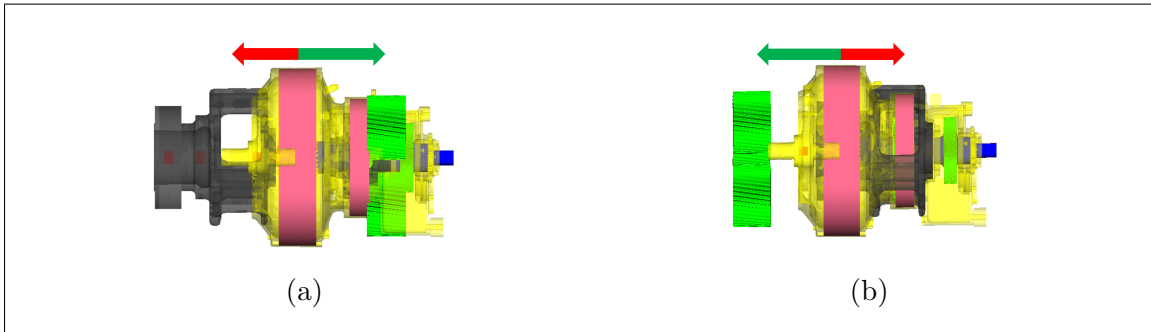


Figure 3.12: Mode 4 first stage planet thrust (1p thrust)

Mode 5 shown in Figure 3.13 is a relatively small whirling mode of the main carrier that *does not* thrust the planet gears.

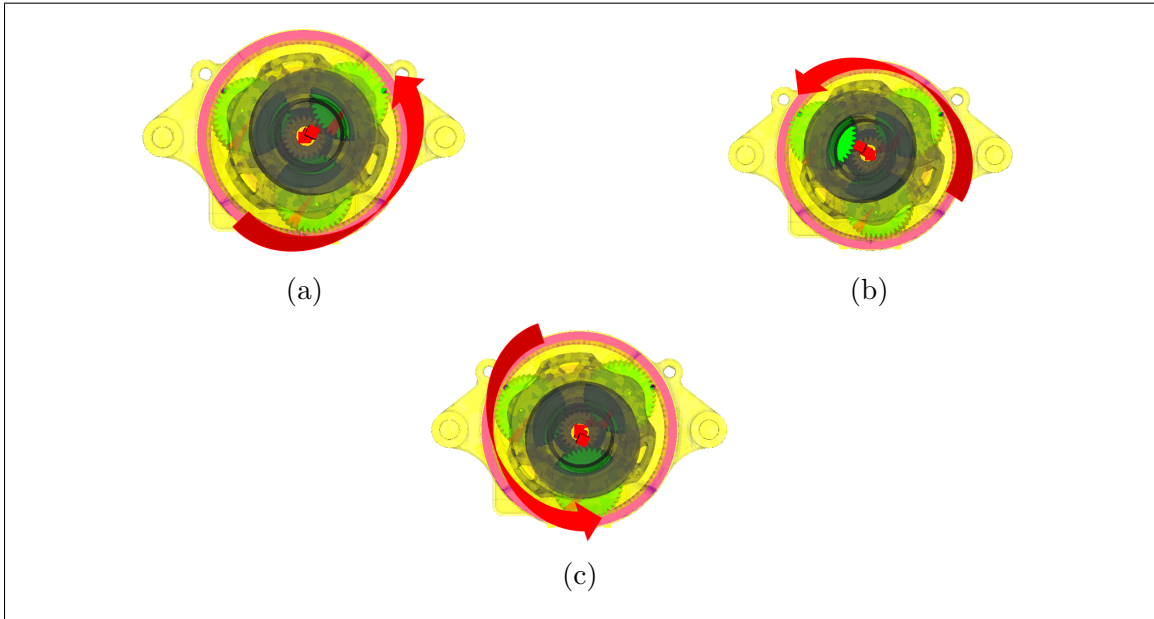
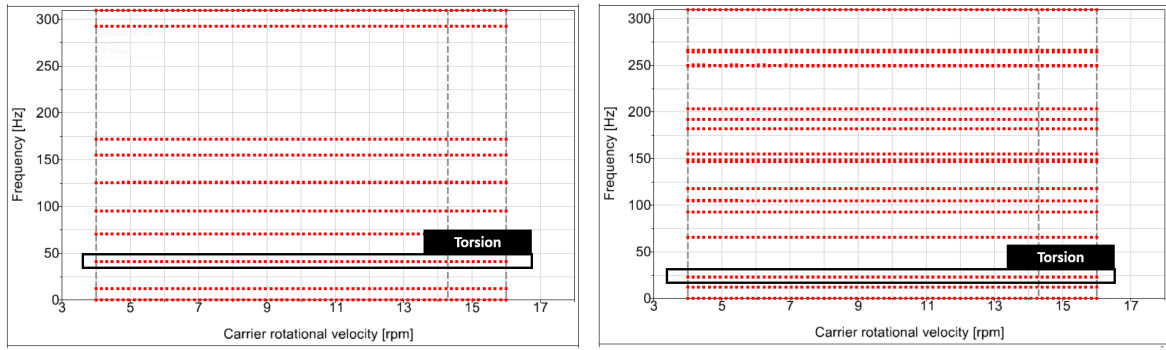


Figure 3.13: Mode 5 first stage carrier whirl (1c whirl)

3.3.3 Results

All configurations showed a horizontal pattern of frequency markers in the low-frequency modes, that is, they are independent of input speed. Figure 3.14 shows the effect of increasing model fidelity on system natural frequencies. The five lowest modes common to all configurations were shifted down as fidelity was increased. The frequency values for the lowest five modes for each configuration are reported below.



(a) Config 1

(b) Config 4

Figure 3.14: Fidelity influence on gearbox natural frequencies

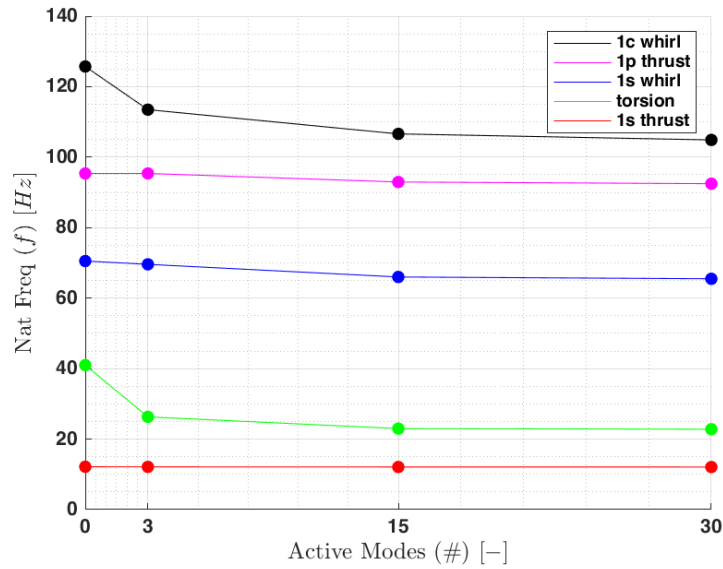


Figure 3.15: Overall effect of component mode switching on gearbox natural frequencies

Table 3.3: Overall effect of component mode switching on gearbox natural frequencies (values plotted in Figure 3.15)

<i>config</i>	Carrier	HSG	1s thrust [Hz]	torsion [Hz]	1s whirl [Hz]	1p thrust [Hz]	1c whirl [Hz]
1		0	12.16	40.99	70.53	95.38	125.73
2		3	12.12	26.31	69.59	95.38	113.48
3		15	12.09	22.99	66.00	92.95	106.60
4		30	12.08	22.80	65.49	92.47	104.89

The graph labels in Figure 3.15 come from the mode shape names in the figure captions of section 3.3.2. Increasing from a rigid model to a low fidelity model affects the main carrier whirl and torsional modes most significantly, while the other system modes experience relatively little shift. The 1c whirl mode sees the most significant decline when moving from low to medium fidelity. The 1p thrust mode experience its first real decline at medium fidelity, suggesting there's a body mode in that range that lowers the stiffness around the main carrier and planet bearings. The torsional frequency shift is more gradual in this range, and is seen to level off when switching from medium to high fidelity. At the same time main carrier whirl still sees significant softening.

It's clear that a rigid model does not capture the correct natural frequencies. The low-fidelity model predicts the first five natural frequencies within 10% of the high-fidelity values. The greatest frequency drop due to model fidelity is in the system's torsional mode which drops almost 15 Hz between the rigid and low fidelity models. Thrusting modes (1s thrust and 1p thrust) were the least impacted. Further softening of the main carrier whirl mode may still be observed in a higher fidelity model in which more modes were extracted in new flexible body CMS models.

3.4 Non-uniform activation of component mode shapes

Configurations summarized in Table 3.4 were prepared in which one body's fidelity varied between low, medium, and high while the other body's fidelity was held high. The first five natural frequencies from these configurations will reveal the relative influence of each body's structural fidelity on system-level modes. Once again, the CMS method made a total of 30 modes available so high-fidelity configurations with 30 modes will be considered to return the true response. 15 modes were selected as a medium fidelity configuration halfway between rigid-body and high-fidelity configurations. 3 modes were selected as the low fidelity configuration because these modes are sufficient to represent the first three bending modes in the housing and carrier.

Table 3.4: Model configurations for studying non-uniform mode activation

<i>config</i>	# Carrier modes	# HSG modes
5	0	30
6	3	30
7	15	30
8	30	0
9	30	3
10	30	15

3.4.1 Results

The lowest natural frequencies of the gearbox system were found to vary with structural fidelity of the housing and carrier. Figure 3.16 shows the natural frequency variation due to the housing alone, and Figure 3.17 shows the variation due to the

carrier alone. Reading right-to-left in the figures effectively shows the sacrifice of accuracy when using lower fidelity models. These bodies do not play equal roles, but their independent effects on the natural frequencies compound on each other resulting in the overall effects seen in Figure 3.15. A rigid housing provides a reasonably good estimation of the high-fidelity natural frequencies, except for the 1c whirl mode. 1c whirl decreases by about 5 Hz, which is a less dramatic drop than was seen in the previous study. Interestingly the 1c whirl frequency drop due to housing fidelity isn't seen until the 3rd-15th housing modes are activated. Torsion is hardly changed by housing fidelity. This is likely because the carrier bearings mounted to the housing transfer housing elastic motion to the carrier.

The torsional mode frequency is much more sensitive to carrier fidelity. 1c whirl drops by 9 Hz from rigid-high fidelity, with its most significant drop due to the carrier's 1st-3rd modes. Note that the housing's influence on 1c whirl was seen most between its 3rd-15th modes. The carrier is responsible for softening both 1s whirl and 1c whirl frequency between low-medium fidelity. Overall the carrier has the greatest impact on the 5 low-frequency modes considered here.

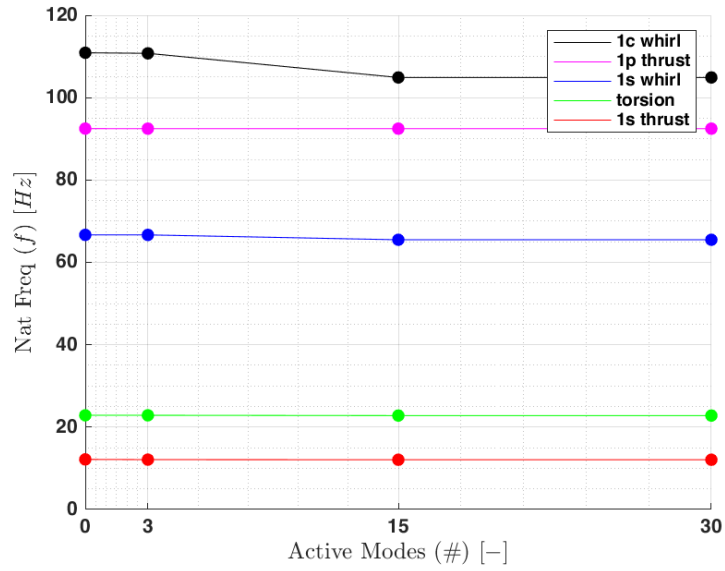


Figure 3.16: Effect of housing mode switching on gearbox natural frequencies

Table 3.5: Effect of housing mode switching on gearbox natural frequencies (values plotted in Figure 3.16)

<i>config</i>	Carrier	HSG	1s thrust [Hz]	torsion [Hz]	1s whirl [Hz]	1p thrust [Hz]	1c whirl [Hz]
8	30	0	12.16	22.87	66.68	92.48	110.89
9	30	3	12.11	22.87	66.67	92.47	110.76
10	30	15	12.09	22.87	65.79	92.47	106.06
4	30	30	12.08	22.80	65.49	92.47	104.89

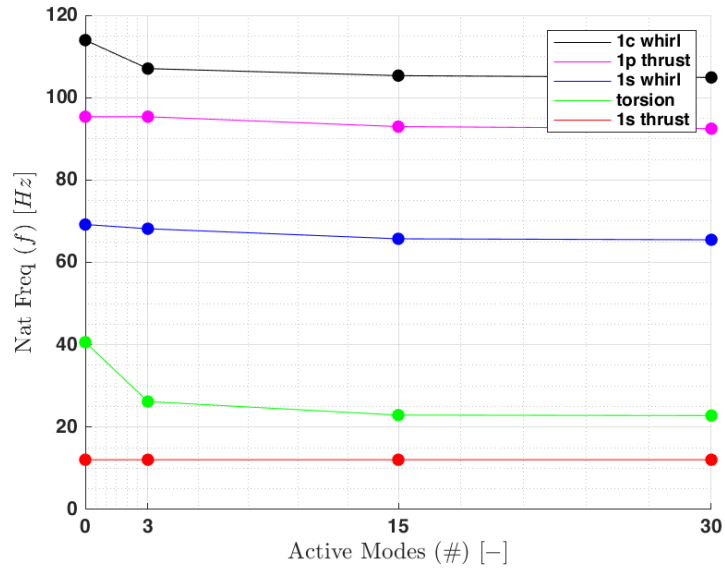


Figure 3.17: Effect of carrier mode switching on gearbox natural frequencies

Table 3.6: Effect of housing mode switching on gearbox natural frequencies (values plotted in Figure 3.17)

<i>config</i>	Carrier	HSG	1s thrust [Hz]	torsion [Hz]	1s whirl [Hz]	1p thrust [Hz]	1c whirl [Hz]
5	0	30	12.08	40.62	69.19	95.37	113.96
6	3	30	12.08	26.21	68.17	95.37	107.05
7	15	30	12.08	22.92	65.72	92.97	105.34
4	30	30	12.08	22.80	65.49	92.47	104.89

Chapter 4

Effect of component flexibility on gearbox risk frequency prediction

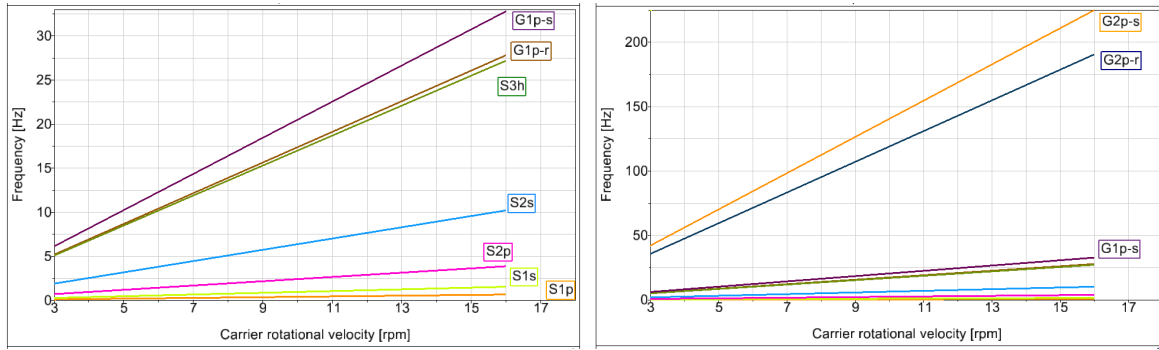
Vibrations in rotor systems are observed during operation by acceleration sensors as indicated by frequency spikes. If resonance is measured at a known risk frequency, the system is said to have reached a *critical speed*. Critical speeds occur when a system natural frequency is excited by internal forces due to imbalance in the system. Critical speed excitation differs from normal resonance which is directly caused by an input forcing frequency matching the system's natural frequency. Machines are designed to operate without crossing critical speeds whenever possible. However if the machine is required to pass these critical speeds it should do so quickly and rarely [12].

Turbine MBS models need sufficient fidelity to accurately predict risk frequencies. Previous work in Chapter 3 introduced a standalone gearbox model and characterized the influence of that model's fidelity on low-frequency modes. This study will investigate the impact of model fidelity on high-frequency vibration of the output shaft. This vibration has the potential to be excited by forces generated inside

the gearbox, which can in turn wear out the high-speed bearing. Output shaft whirl vibration is different from previous gearbox modes discussed in Chapter 3 because this mode shows speed-dependence. The method of Campbell analysis will prove useful in evaluating how model fidelity impacts rotor behavior and potential excitation of the whirl mode.

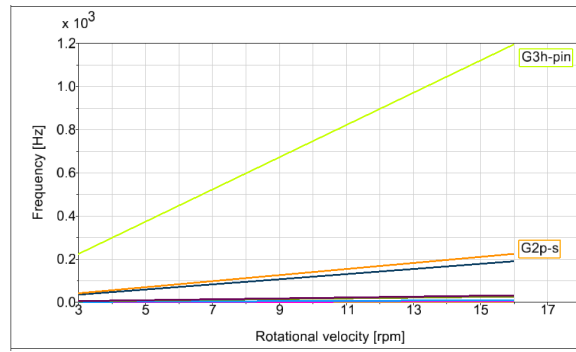
4.1 Campbell analysis

Campbell analysis is a method for analyzing rotor dynamic systems to find critical speeds. The first step in Campbell analysis is to take account of all rotor speeds. Plotting these rotor speeds on a 2D Campbell diagram will highlight specific components that have the potential to match system natural frequencies, and at what frequency that excitation could occur. The first step of Campbell analysis can seem overwhelming for this gearbox because it is a complex system by virtue of its multiple stages with shafts and gears moving at different speeds. A simple way to conceptualize all these moving parts is to find how each component's rotation relates to the input rotation. For example, when the main carrier rotates at 4 rpm, another gearbox component may be found to rotate twice as fast at 8 rpm. That component is said to be of order 2, and if it rotated three times as fast as input it would be order 3, and so on. The orders for all shaft rotations and gear meshes in the gearbox system are visualized in Figure 4.1 as functions of the main carrier rotation.



(a) Low orders

(b) Medium orders



(c) High orders

Figure 4.1: Gear and shaft orders

Table 4.1: Order line labels

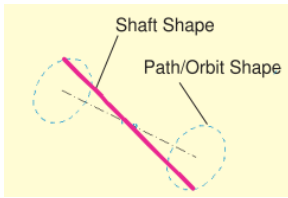
S1p: First stage planetary shaft	G1p-r: First stage planet-ring mesh
S1s: First stage sun shaft	G1p-s: First stage planet-sun mesh
S2p: Second stage planet shaft	G2p-r: Second stage planet-ring mesh
S2s: Second stage sun shaft	G2p-s: Second stage planet-sun mesh
S3h: Third stage helical shaft	G3h-pin: Third stage helical-pinion mesh

If you were to graph these order lines on top of the system natural frequency charts such as Figure 3.8, some of the order lines would intersect natural frequencies. The frequency at a given intersection is called a *risk frequency*. The risk is that an im-

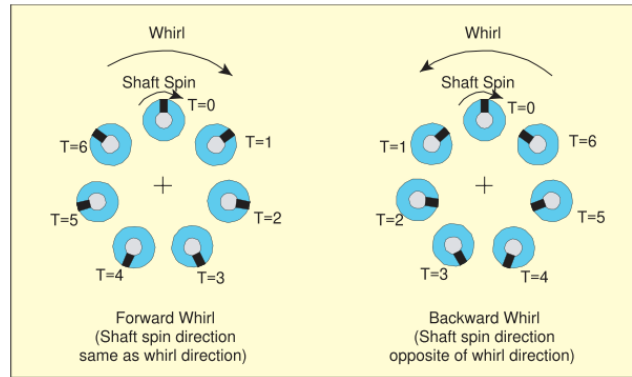
balance in the corresponding gearbox component can generate internal forces, which could in turn excite the system's natural frequency [12]. Imbalance can be caused by an unequal distribution of mass on a single body, or asymmetric applied forces that misalign shafts or gears. For example, configuration 4 in Chapter 3 predicted a 1s thrust mode at 12.08 Hz. The max speed of the main carrier is 16 rpm (1.67 Hz) so imbalance transmitted by the main carrier could never oscillate at the 12.08 Hz thrust frequency. Thus, the carrier is not at risk of exciting this mode. However, there are other components in the gearbox moving at higher speeds than the main carrier. This method of Campbell analysis is necessary to reveal what components can excite gearbox modes, and at what frequency those excitations might occur.

4.1.1 Output shaft whirl mode

Conical whirl is a common vibration excited by rotor system imbalance. This mode shape is so-called because the path traced out by a whirling shaft forms a cone shape. The whirling motion can be visualized as a shaft pitching back and forth toward its nose, and then caused to spin bringing it into orbit. This mode is observed in the turbine gearbox at the output shaft, and this mode was chosen for investigation because it exhibits speed-dependence that other modes did not. Also, this mode vibrates the failure-prone high-speed area of the gearbox, which may contribute to the accelerated bearing wear. Whirl generally comes in forward and backward senses as shown in Figure 4.2.



(a) Conical whirl orbit path



(b) Forward & backward whirl

Figure 4.2: Conical whirl [12]

Whirling forward means that the conical orbit advances in the same direction that the shaft spins, while backward whirl orbits in the opposite direction of shaft spin. The pitching nature of conical whirl introduces gyroscopic effects. As shaft speed increases, the gyroscopic effect essentially acts like an increasingly stiff spring on the shaft, increasing forward whirl frequency. The opposite is true for backward whirl; increasing shaft speed softens backward whirl frequency [12].

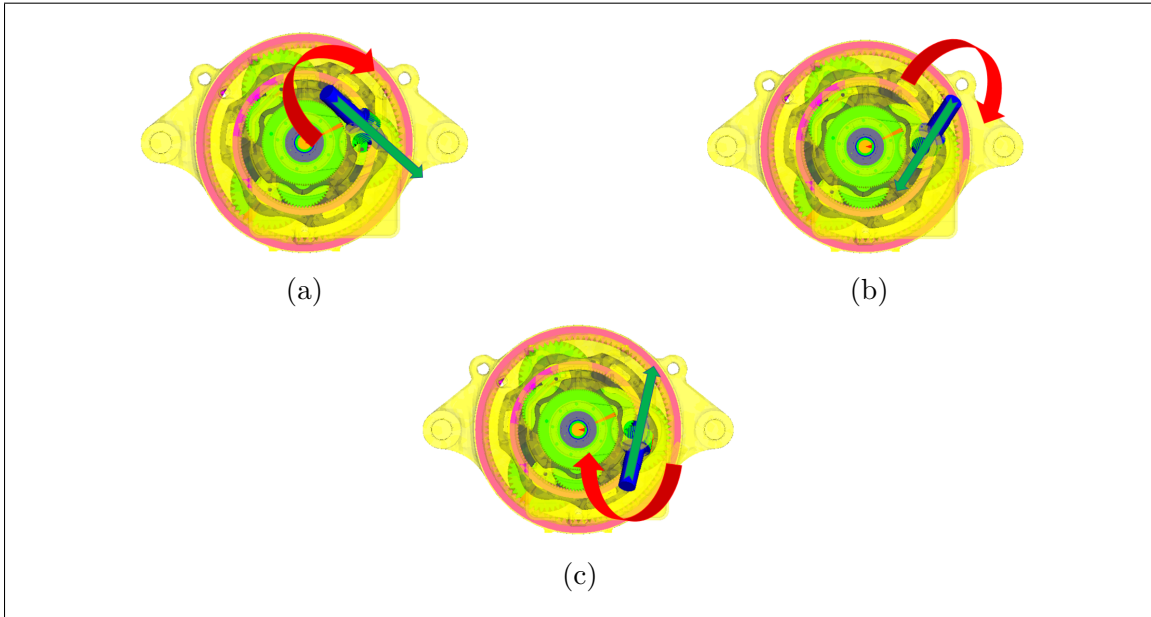
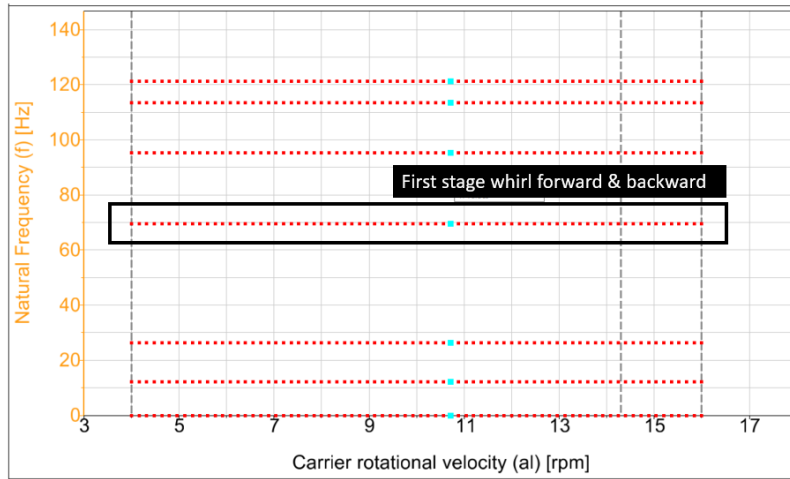
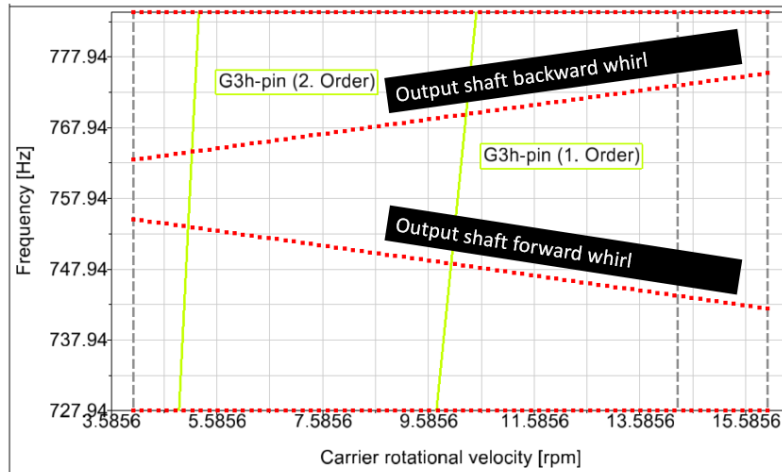


Figure 4.3: Output shaft forward conical whirl (red arrow is whirl direction; green arrow is shaft spin direction according to right hand rule)

Figure 4.3 shows the output shaft spinning clockwise (green arrow) while orbiting clockwise (red arrow), so this is forward whirl. Output shaft whirl is excited at a relatively high frequency on the order of 700 Hz. The gyroscopic effect causes the natural frequencies of whirl to diverge, unlike first stage whirl where the forward/backward frequencies were roughly equal and do not change with shaft speed.



(a) First stage carrier whirl (no gyroscopic effect)



(b) Output shaft whirl (has gyroscopic effect)

Figure 4.4: Gyroscopic effect on whirl frequency

Forward whirl is known to increase in frequency with increasing shaft speed due to the gyroscopic effect, but Figure 4.4 shows forward whirl decreasing with shaft speed. Backward whirl frequency is known to decrease, but in Figure 4.4 it rises. This inversion of backward/forward whirl behavior was observed in Simpack models of even the simplest multi-DOF Jeffcott rotor (see Appendix B). A thorough search did not reveal a modeling error that is known to cause this inversion of backward/forward whirl. The investigation of fidelity influence was carried on despite this known error.

It was assumed that if the inversion of backward/forward whirl was resolved the values of frequency would be roughly the same. Therefore, conclusions based on whirl frequency can still hold true despite these mode shapes being predicted in the wrong order.

4.2 Uniform activation of component mode shapes

The standalone gearbox was used to make the model configurations in Table 4.2 which were studied using Campbell analysis (configurations from section 3.3.1 were used again). The configurations vary uniformly in the structural fidelity used on the carrier and housing bodies. The gearbox was first equilibrated with gravity absent any input torques. Then torque was simultaneously applied to the main carrier and output shaft driving the system up to an operating speed of 16 rpm. These configurations will be analyzed to observe the overall effect of model fidelity on the output of interest- the risk frequency for output shaft whirl.

Table 4.2: Model configurations for studying uniform mode activation

<i>config</i>	<i>fidelity</i>	# Carrier modes	# HSG modes
1	Rigid	0	0
2	Low	3	3
3	Medium	15	15
4	High	30	30

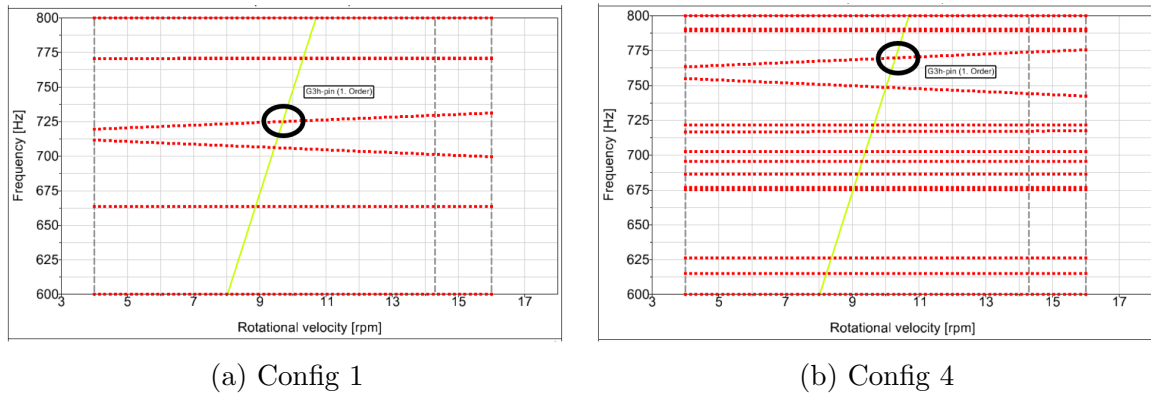


Figure 4.5: Fidelity influence on whirl excitation via pinion gear mesh

Model fidelity changed the risk frequency where third stage helical-pinion gear mesh could excite backward conical whirl. Figure 4.5 shows that increasing fidelity activated system modes that didn't appear in a rigid-body system. The critical observation from Figure 4.5 is the shift of the black circle highlighting a rise in whirl frequency. The whirl risk frequency was recorded for the different gearbox fidelity levels and reported below.

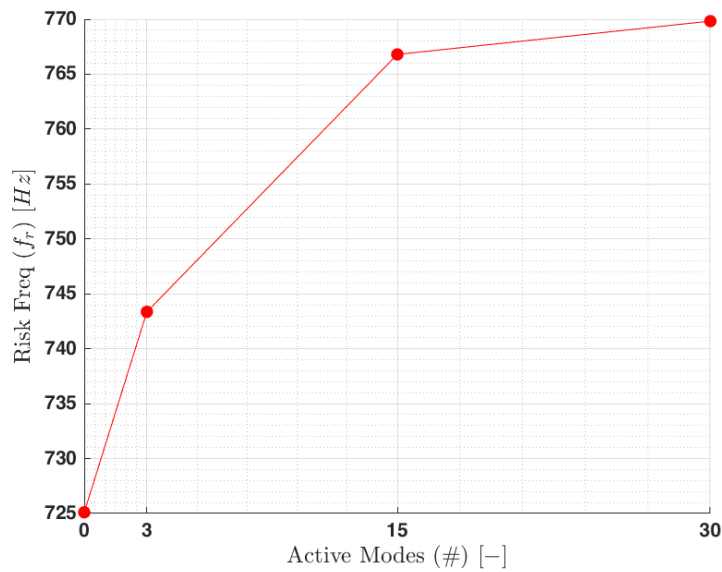


Figure 4.6: Overall effect of component mode switching on whirl risk frequency

Table 4.3: Overall effect of component mode switching on backward whirl risk frequency (values plotted in Figure 4.6)

<i>config</i>	Carrier	HSG	Risk f [Hz]
1		0	725.11
2		3	743.36
3		15	766.80
4		30	769.83

The results in Figure 4.6 report the intersection point of the pinion gear mesh order with the speed-varying backward whirl mode of the output shaft. Model fidelity strongly shifted the whirl risk frequency with the greatest difference of 45 Hz observed between rigid to high fidelity configurations. The frequency shift from low to medium fidelity was greater than the frequency shift from medium to high fidelity. Risk frequency predicted with a medium fidelity model is converges within 3 Hz (1%) of the high-fidelity risk frequency. Since frequency shifts on the order of 3 Hz are significant in dynamic design considerations, more flexibility in gearbox components is warranted to accurately assess the whirl mode. It remains to be seen whether the housing or the carrier is contributing to this shift. Either component's mode shapes could reasonably interact with output shaft whirl.

4.3 Non-uniform activation of component mode shapes

The standalone gearbox was used to make the model configurations in Table 4.4 which were studied using Campbell analysis (the same configurations chosen in section 3.4 were used again). The configurations vary non-uniformly in the number of active body modes assigned to the carrier and housing. The same simulation

procedure described in the previous section was followed. These configurations are interesting once again because they will reveal the independent contributions of the main carrier and housing on the speed-dependent whirl risk frequency.

Table 4.4: Model configurations for studying non-uniform mode activation

<i>config</i>	# Carrier modes	# HSG modes
5	0	30
6	3	30
7	15	30
8	30	0
9	30	3
10	30	15

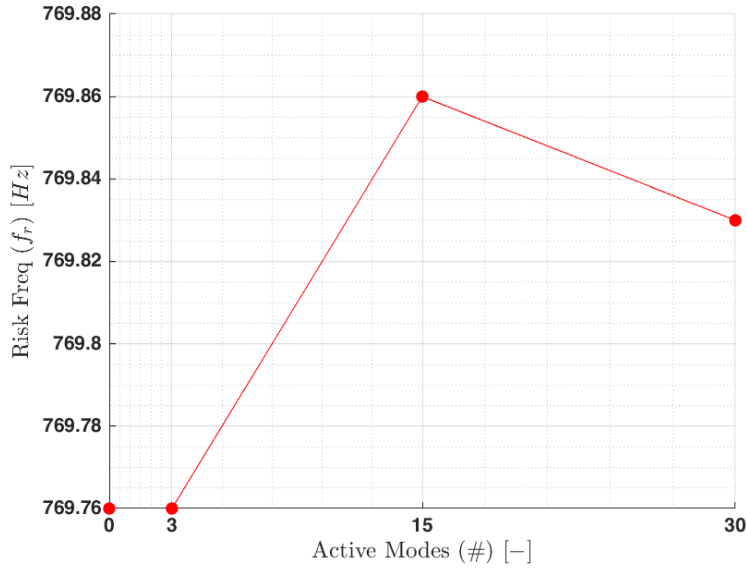


Figure 4.7: Effect of carrier mode switching on whirl risk frequency

Table 4.5: Effect of housing mode switching on whirl risk frequency (values plotted in Figure 4.7)

<i>config</i>	Carrier	HSG	Risk f [Hz]
5	0	30	769.76
6	3	30	769.76
7	15	30	769.86
4	30	30	769.83

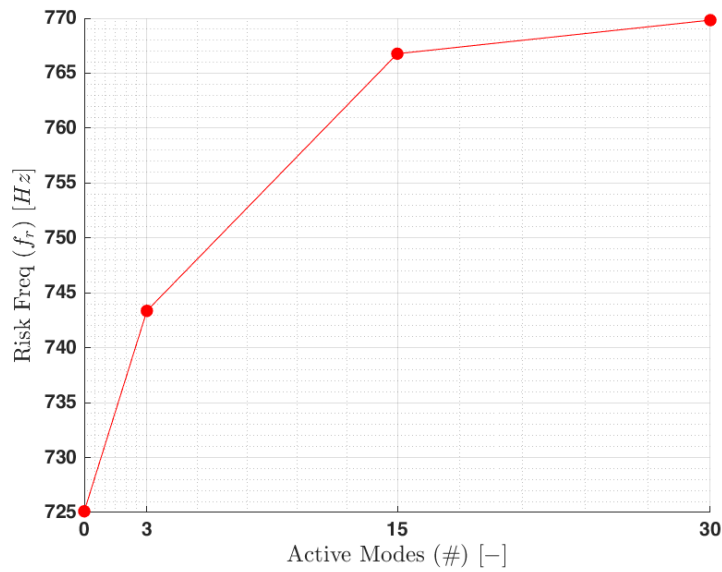


Figure 4.8: Effect of housing mode switching on whirl risk frequency

Table 4.6: Effect of housing mode switching on whirl risk frequency (values plotted in Figure 4.8)

<i>config</i>	Carrier	HSG	Risk f [Hz]
8	30	0	725.11
9	30	3	743.36
10	30	15	766.77
4	30	30	769.83

Figure 4.7 reveals that the carrier body modes have very little impact on risk

frequency- only 0.7 Hz difference between the rigid to high fidelity configurations. Figure 4.8 shows that the housing is the primary cause of the shift in whirl frequency. This is likely because the flexing motion of the front housing feeds directly to the output shaft's bearings through the rear housing. Although it's possible that the housing interacts with the output shaft by way of its connection to the first stage ring, which is related to the first stage sun shaft, which in turn is rigidly fixed to the second carrier, and eventually to the output shaft. Returning to Figure 4.5 shows that high fidelity models not only predict higher whirl frequency, but the divergence between forward/backward whirl is also stronger. If the modeling objective centers on the output shaft whirl mode, it would be more computationally effective to leave the carrier in a low fidelity representation and add more than 30 modes to the housing body. Upgrading from 30 to 45 housing modes could reasonably cause another frequency shift on the order of 1 Hz.

Chapter 5

Conclusions

An initial review of EIC's turbine drivetrain model motivated separate investigations of the influence of model fidelity as measured by reactions both internal and external to the gearbox. A method has been proposed for judging the influence of various aspects of MBS model fidelity. The investigations involved preparing models with various structural and gearbox fidelities and running these models through load sequences to measure their relative performance.

Structural fidelity was studied by replacing some rigid body components with flexible bodies. The most important finding in this study was that models with rigid components had underestimate the true radial misalignment at the gearbox side of the high-speed shaft coupling by as much as 94%. Upgrading rigid components models with 3 modes of flexibility will require 3.78x more solve time, and upgrading to models with 30 modes of flexibility will require 5x solve time. Out of four rigid components that were replaced by flexible members, the bed plate is the most significant flexible body affecting motion at the high-speed shaft. Low-frequency modes of the standalone gearbox are softened as model fidelity increased, most significantly in torsion and whirl modes, while thrusting modes saw little change. In the high-frequency range

increasing model fidelity caused the output shaft whirl frequency to shift up by as much as 45 *Hz*.

Chapter 6

Future work

The most important next step is to compare model output documented here with test data measured during EIC drivetrain experiments. Yet a model such as the one developed here can support design analytics that would be very difficult or impossible to achieve accurately in the lab. For example, the gear tooth force information available in Simpack could inform the design of a precise gear tooth geometry optimized for a certain load level. Next steps in the current investigation will be to carry out a focused study of risk frequencies in the high-speed area of the standalone gearbox. These risk frequencies can be analyzed using the 3D Campbell analysis module in Simpack. An imbalance would need to first be created by applying a yaw or nod force in the system, likely at the main carrier. Another imbalance could be created by attaching an artificial mass to shafts and/or gears, or misaligning a connection element. Frequency peaks on a 3D Campbell order chart will confirm which risk frequencies are being excited.

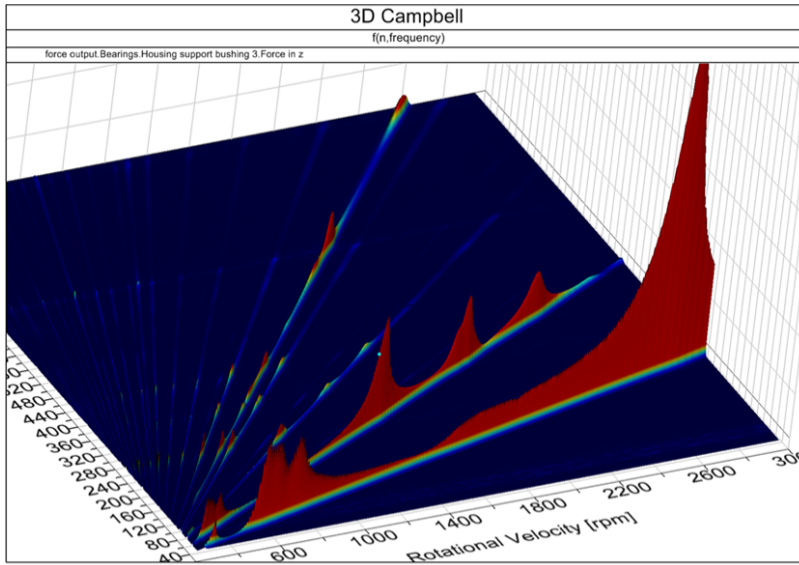


Figure 6.1: Example of 3D Campbell chart [7]

Simpack allows use of higher fidelities for bearings and gear forces than the ones used in the current study (see Appendix A discussing why FE 225 was left out). Simpact offers special force elements to model roller bearings, and the addition of microgeometries to the gears etc. The choice of which modeling elements to study next will be limited to the quality of physical data available to parametrize them.

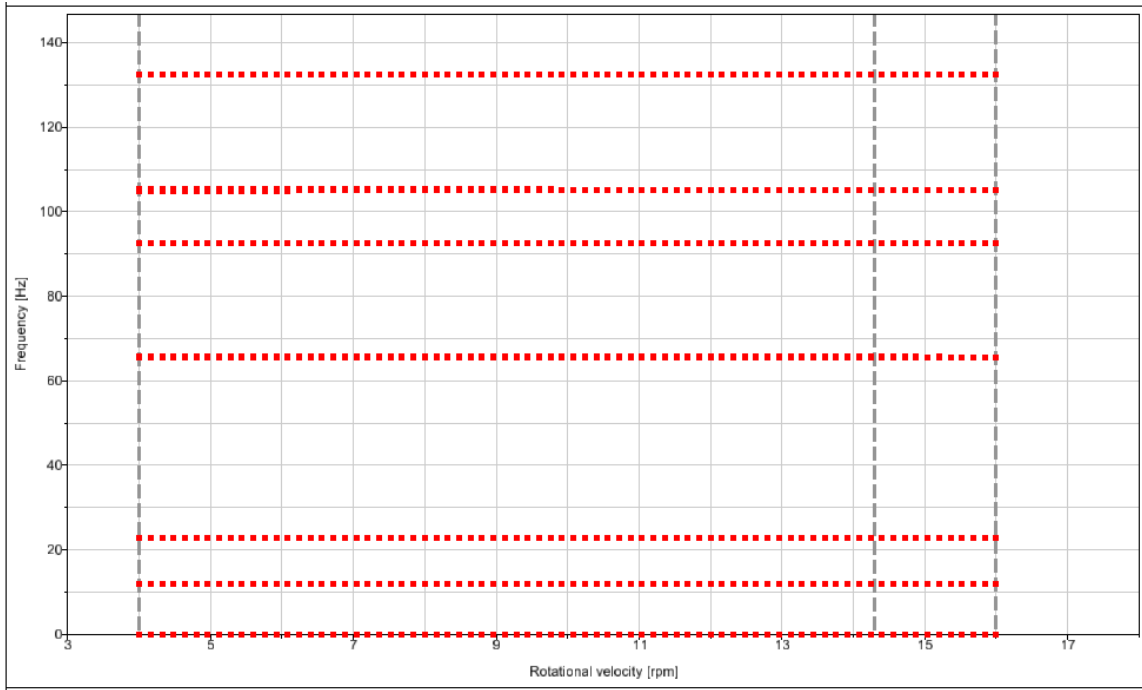
Project partners have expressed interest in refining the overall machine head model. Attention may turn to the main shaft bearing, making use of dynamic loads that emulate true wind conditions for validation with testbench data. This study showed the opportunity to improve accuracy by processing FE models to include more modes in the four flexible bodies. Gearbox natural frequencies such as main carrier whirl will likely still see more frequency shifts when these new modes are extracted. There are plenty of other interesting reactions to characterize throughout the high-fidelity gear train especially related to gear meshing. The overwhelming advantage of MBS modes such as this one is that virtually all kinematic or kinetic

information that one might need is easily available.

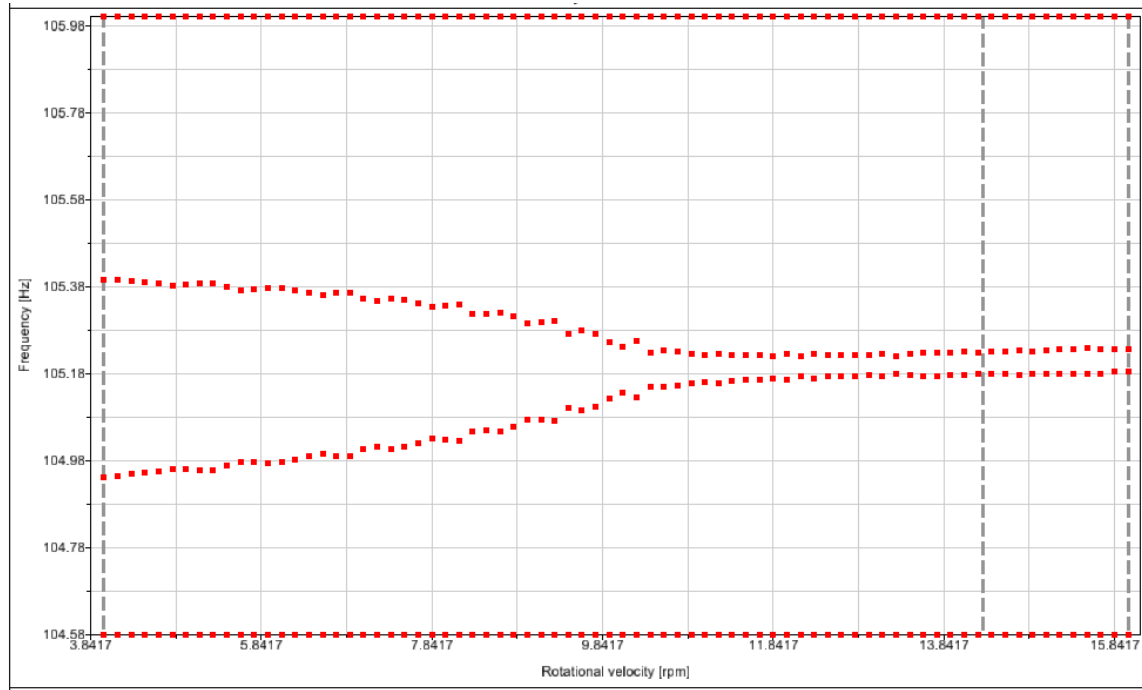
Appendices

Appendix A Natural frequency fluctuations using FE 225

Figures 2 and 3 are 2D Campbell charts of standalone gearbox model runup to 16 rpm. They are essentially the same model except for that one model uses gear element 204 and the other uses element 225 to represent gear meshing. The same gear geometry, material, stiffness, and backlash information were used in all gear elements. Models using FE 225 exhibited 3 Hz fluctuations in the 5th natural frequency corresponding to first stage carrier whirl vibration. Models using FE 204 showed more normal monotonic changes in natural frequencies, albeit very small changes. While FE 225 should be desirable for future modeling work, especially when meshing excitations and gear micro geometry effects are important, FE 225 is the correct model to use. This mode, and any other fluctuating modes, should be investigated and diagnosed before FE 225 is carried forward and used in 3D Campbell analysis.

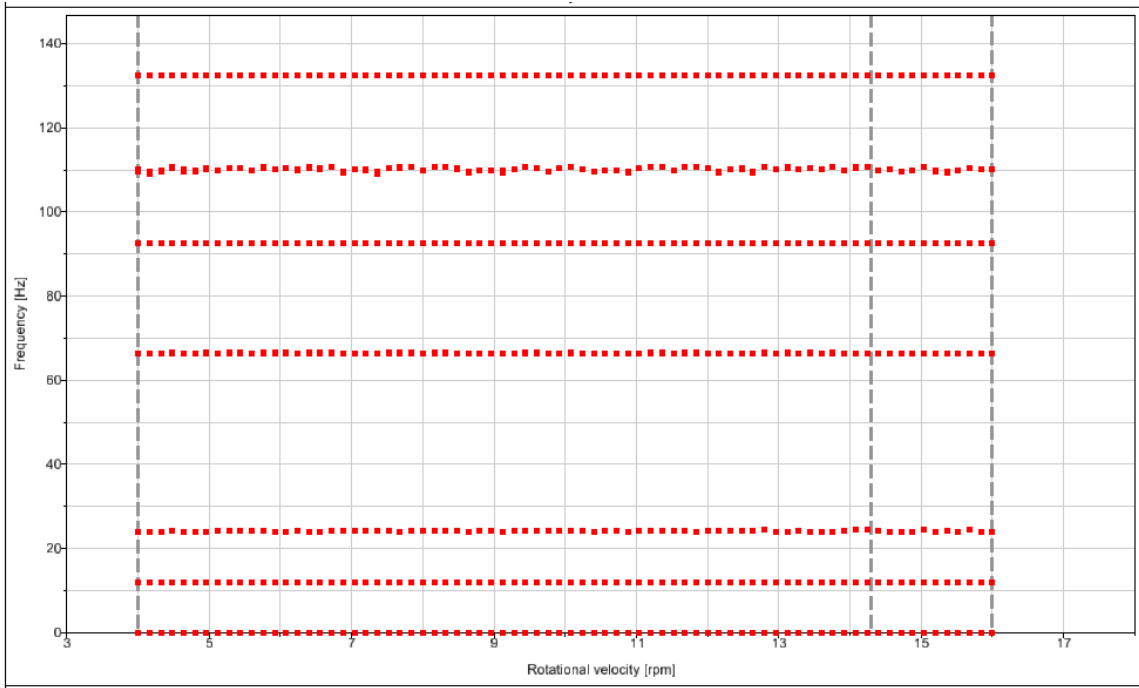


(a) FE 204 system frequency chart

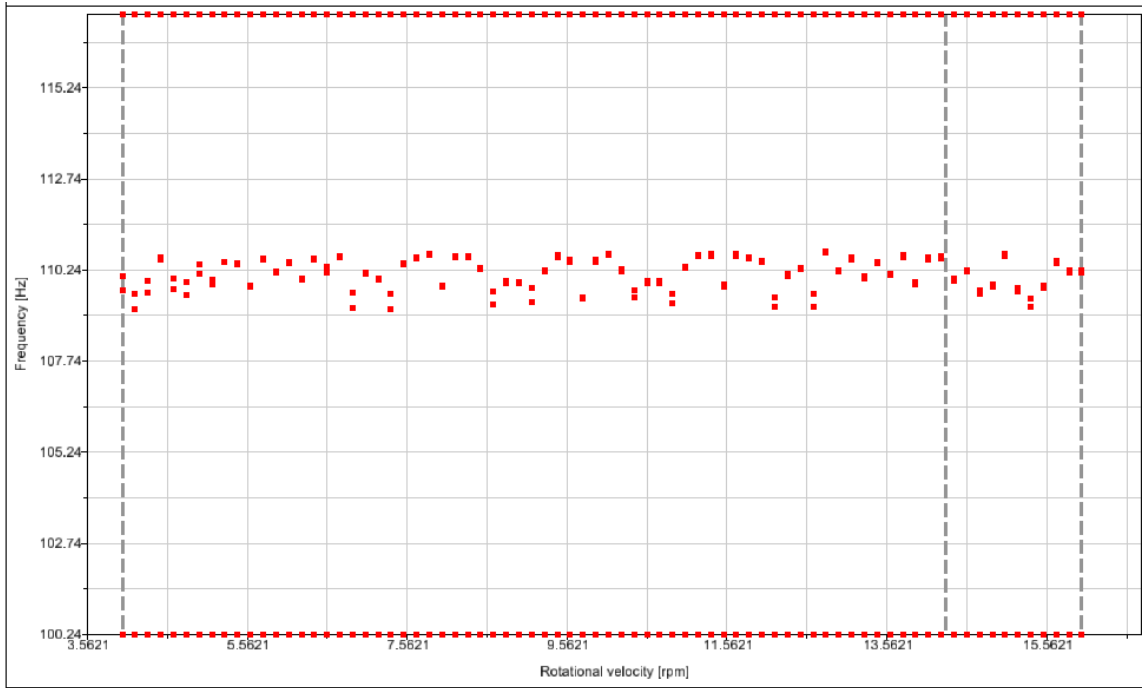


(b) Zoomed

Figure 2: FE 2040 monotonic system frequency chart



(a) FE 225 system frequency chart



(b) Zoomed

Figure 3: FE 225 Fluctuations in 2D Campbell chart

Appendix B Simple Multi DOF Jeffcott Rotor

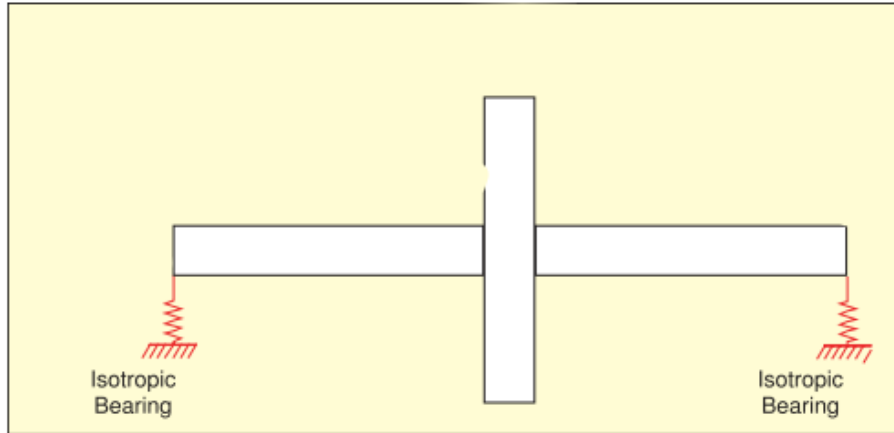


Figure 4: Multi DOF [12]

A multi-DOF Jeffcott rotor model was prepared according to the suggested design discussed by Swanson [12]. The model has mass and geometry parameters reported below that emulate the scale and inertia of the gearbox output shaft, but the center hung mass is larger and heavier than the pinion gear.

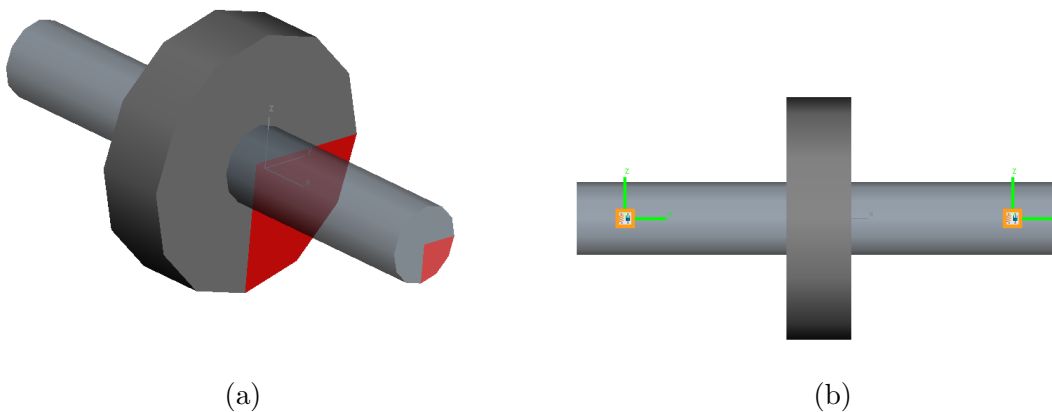


Figure 5: Multi DOF Jeffcott rotor model

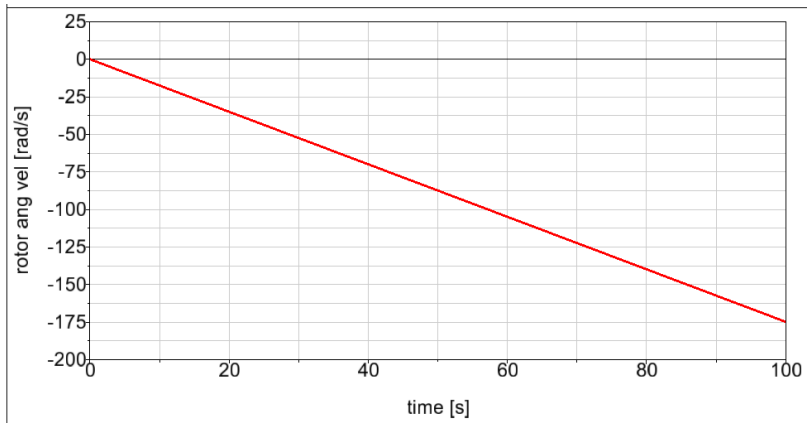


Figure 7: Linear runup of Jeffcott rotor

Modal analysis revealed two whirling modes of the rotor.

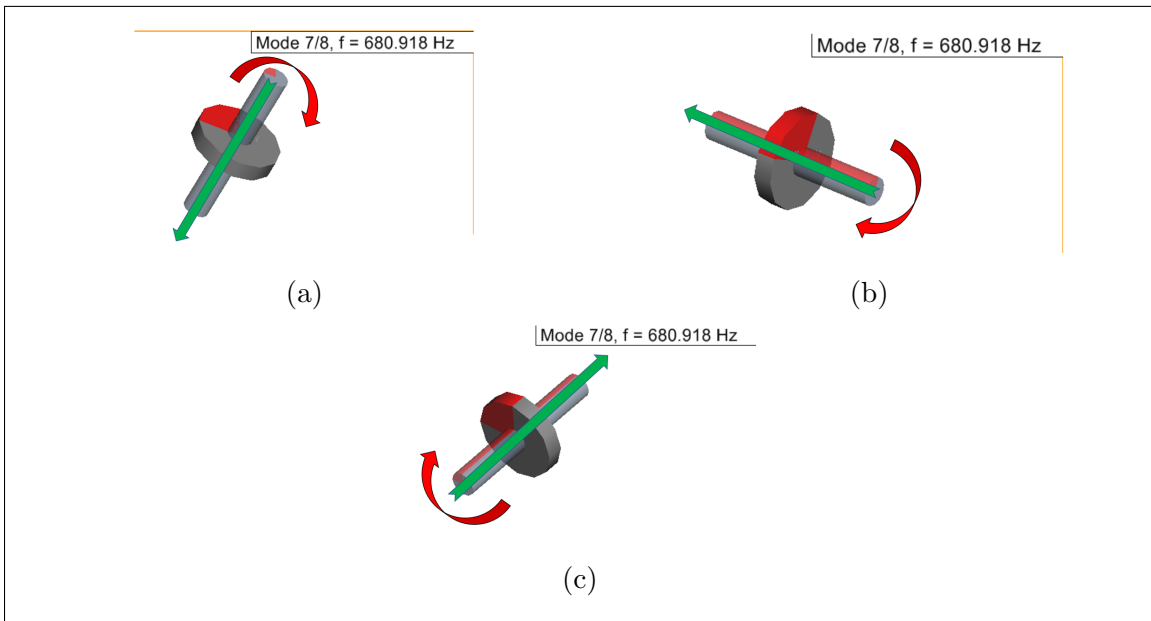


Figure 8: Forward whirl mode shape

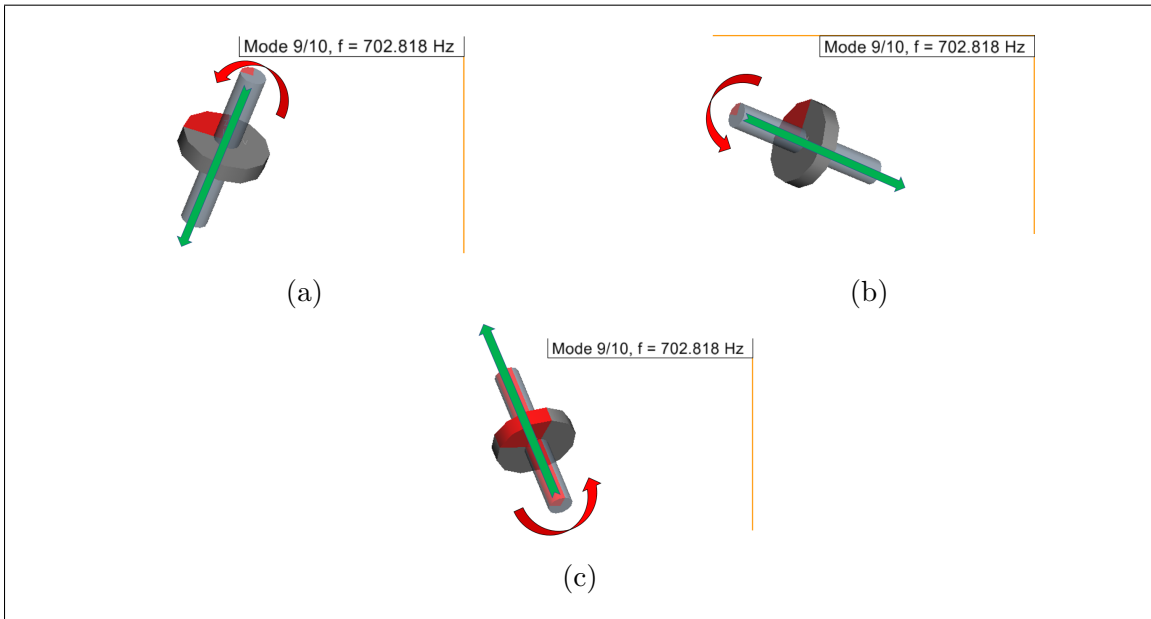


Figure 9: Backward whirl mode shape (red arrow is whirl direction; green arrow is shaft spin direction according to right hand rule)

The forward whirl is observed 22 Hz below backward whirl. The forward mode should be observed higher than the backward mode, and should increase with rotor speed. Understanding how this forward/backward whirl inversion arises from a simple MBS system such as this will shed light on the output's shaft forward/backward whirl in the standalone gearbox.

Bibliography

- [1] N. Beasley and J. Thakkar. Drivetrain characterization of wind turbine platform. Technical report, 03 2019.
- [2] J. Betran, A. Heege, and Y. Radovic. Fatigue load computation of wind turbine gearboxes by coupled finite element, multi-body system and aerodynamic analysis. *Wind Energy*, 10(5):395–413, 2007.
- [3] S. Butterfield, B. McNiff, and W. Musial. Improving wind turbine gearbox reliability. Technical report, National Renewable Energy Lab.(NREL), Golden, CO (United States), 2007.
- [4] Energy Innovation Center. 7.5 mw test rig. <https://clemsoneenergy.com/wind-turbine-test-beds/>.
- [5] Energy Innovation Center. About the center. <https://clemsoneenergy.com/about/>.
- [6] Dassault Systemes Simulia Corp. *Simpack Documentation*. 2017.
- [7] Dassault Systemes Simulia Corp. *Simpack Drivetrain Tutorial*. 2017.
- [8] W. Desmet, J. Helsen, B. Marrant, F. Vanhollebeke, and D. Vandepitte. Multi-body modelling of varying complexity for modal behaviour analysis of wind turbine gearboxes. *Renewable Energy*, 36(11):3098–3113, 2011.
- [9] M. Froese. Lessons learned lead to new ideas in gearbox bearings. *Windpower Engineering and Development*, 2017.
- [10] B. Gould, A. Grecco, and J. Keller. Investigation of Bearing Axial Cracking : Benchtop and Full- Scale Test Results. (NREL/TP-5000-67523):116, 2017.
- [11] R. Parker. Dynamic Analysis of Planetary Gears With Bearing Clearance. 7(October 2012):1–15, 2019.
- [12] Erik Swanson, Chris D Powell, and Sorin Weissman. A Practical Review of Rotating Machinery Critical Speeds and Modes. *Sound and Vibration*, 39(5):10–17, 2005.